Geothermics 94 (2021) 102094

Contents lists available at ScienceDirect

Geothermics

journal homepage: www.elsevier.com/locate/geothermics

Multiscale short-circuiting mechanisms in multiple fracture enhanced geothermal systems

Bruce Gee [a], Robert Gracie [a,*], Maurice B. Dusseault [b]

[a] Department of Civil and Environmental Engineering, University of Waterloo, Waterloo, Ontario N2L 3G1, Canada
[b] Department of Earth and Environmental Sciences, University of Waterloo, Waterloo, Ontario N2L 3G1, Canada

ARTICLE INFO

Keywords:
Enhanced geothermal
Thermo-hydro-mechanical
Short-circuiting
Multi-fracture

ABSTRACT

Heat extraction from an enhanced geothermal system (EGS) is a complex coupled thermo-hydro-mechanical process. The viability of an EGS is compromised by short-circuiting, a phenomenon resulting from positive thermo-hydro-mechanical feedback loops within the reservoir. In this article, the mechanisms by which short-circuiting occurs in EGSs are studied and described. EGS well doublets are modelled using a fully-coupled thermo-hydro-mechanical finite element model. Flow through the reservoir is restricted to discrete fracture planes, which are hydraulically linked via the injection and production wells. The general behaviour of the system is modelled, starting from the initially distributed flow through the fractures, through to the dominance of flow along a single flow pathway. Both single and multi-fracture EGSs are studied. Short-circuiting is demonstrated to be a multiscale phenomenon, as both in-plane and inter-plane short-circuiting mechanisms are observed. In-plane short-circuiting manifests through flow channeling and, in the studied systems, is the dominant mechanism that controls the production temperature of the system. The behaviour of flow channeling is characterized with four production regimes. It is demonstrated that the effects of flow channeling are more severe in multi-fracture EGSs. Two new inter-plane short-circuiting mechanisms are observed for the first time: plane channeling, and bifurcation of the short-circuiting pathway. The inter-plane mechanisms are demonstrated to have large impacts on the distribution of flow through the reservoir, but are observed to have little effect on the production temperature.

1. Introduction

Enhanced geothermal systems (EGS) are emerging technologies that provide new methods to access energy generated by the radioactive decay within the Earth's crust. Extracting heat from deep rock formations has traditionally required a rock mass that is both naturally hot, porous and permeable, so that hot fluids could be obtained at commercially interesting rates. In an EGS installation (also called a Hot Dry Rock (HDR) installation), access to a hot but low permeability rock mass is enhanced through the use of hydraulic fracturing, creating a fracture network through which fluid can flow. The extracted heat may be used to generate power or for direct heating of homes and businesses (Grasby et al., 2013; Kinney et al., 2019). However, the long-term viability of EGS as a sustainable energy source is impacted by short-circuiting — a natural consequence of the positive feedback loop created by thermo-hydro-mechanical interaction within the rock mass. This article seeks to further understand the process of short-circuiting within an EGS.

Fig. 1 shows a diagram of an EGS well doublet (one injection and one production well) in which the wells are hydraulically connected by large planar fractures. There are many interacting processes within a geothermal reservoir, including: heat transfer within and between the rock mass and working fluid; flow of the working fluid through the rock mass; and, deformation of the rock mass. Thus, EGS models must be coupled and multi-physics.

Much work has been done exploring the behaviour of EGS systems. Existing work can largely be categorized according to: (a) whether or not deformations are considered, subdividing existing models into thermo-hydro (TH) models and thermo-hydro-mechanical (THM) models; and (b) the nature of the fluid flow model. Fluid flow models can be generally subdivided as continuum flow, network flow, or dominant fracture flow. Continuum flow idealizes the fractured rock mass as a porous continuum through which the fluid flows. TH continuum models include the works of Zeng et al. (2013), Aliyu and Chen (2018), and

* Corresponding author.
E-mail addresses: b3gee@uwaterloo.ca (B. Gee), rgracie@uwaterloo.ca (R. Gracie), mauriced@uwaterloo.ca (M.B. Dusseault).

https://doi.org/10.1016/j.geothermics.2021.102094
Received 18 August 2020; Received in revised form 2 February 2021; Accepted 14 March 2021
Available online 26 March 2021

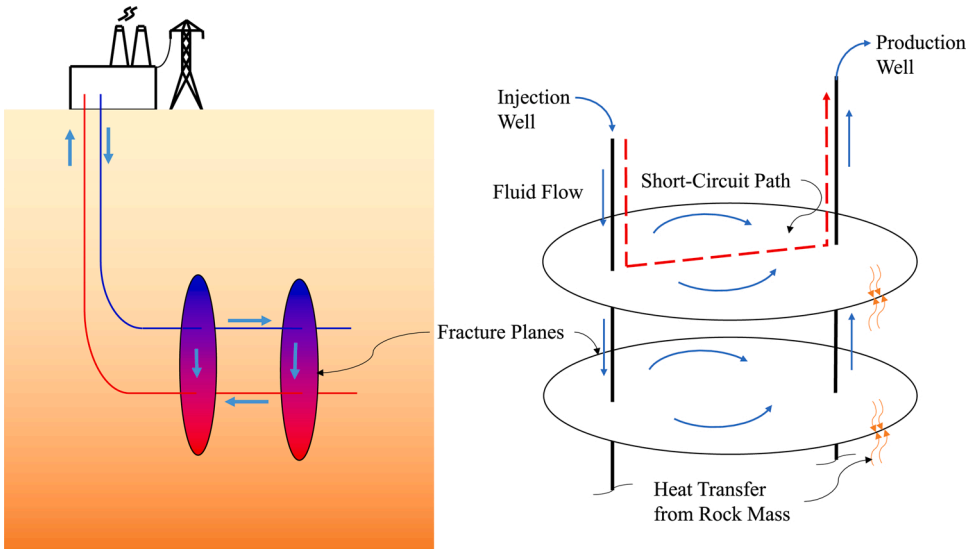

Fig. 1. Schematic of an enhanced geothermal doublet well. The image on the left shows the orientation of the system relative to the surface, while the image on the right shows a close-up schematic of the system and the fluid flow within the system.

Wang et al. (2019a), while THM continuum models include the work of Ghassemi and Zhou (2011), Gan and Elsworth (2016), and Salimzadeh et al. (2018a). Network flow models assume that the wells are linked by a discrete fracture network, which is typically algorithmically generated due to the difficulty in mapping an in-situ fracture network. The network is generated to emulate natural fracture systems that have non-isotropic properties and reflect the presence of different joint sets and their non-orthogonal attitudes. TH network flow models include the works of Shaik et al. (2011) and Chen et al. (2018), while THM network flow models include the works of Fu et al. (2016), Wang et al. (2019b) and Zhang et al. (2019). Lastly, dominant fracture flow models assume that flow within the fractured rock mass is restricted to some number of discrete dominant fracture planes. This flow model is similar to network flow, but simplifies the network to discrete planes which are typically connected to the injection and production wells, but not to each other. This is the assumed EGS flow model adopted for this paper. TH dominant fracture flow models include the works of Mohais et al. (2011) and Xia et al. (2017) for a reservoir featuring a single fracture plane, and the works of Han et al. (2020) and Gong et al. (2020) for multi-fracture reservoirs. THM dominant fracture flow models include the works of Guo et al. (2016), Pandey et al. (2017) and Salimzadeh et al. (2018b) for single fracture plane reservoirs, and the work of Slatlem Vik et al. (2018) for multi-fracture plane reservoirs. Dominant fracture flow models have also been extended to THMC models, in which chemical dissolution is coupled to the THM processes, such as in the work of Salimzadeh and Nick (2019).

Comparison between TH and THM simulations have consistently demonstrated that production temperature decreases faster (and therefore also energy extraction and economic returns) when thermal contraction effects are considered (Fu et al., 2016; Guo et al., 2016; Pandey et al., 2017; Slatlem Vik et al., 2018). Despite this, THM modelling is less common than TH modelling because of the increased modelling complexity and nonlinearity introduced by the mechanical coupling. THM modelling has been used to explore the effects of heterogeneity within an aperture field (Guo et al., 2016) or fracture network (Gan and Elsworth, 2016; Fu et al., 2016; Wang et al., 2019b), as well as the impacts of various parameters such as matrix and joint stiffness (Pandey et al., 2017; Slatlem Vik et al., 2018), and matrix permeability (Salimzadeh et al., 2018a; Pandey et al., 2017). Modelling of multi-fracture planar reservoirs is common in TH models (Han et al., 2020; Gong et al., 2020), but rare among THM models since THM models are more difficult to construct, more computationally expensive, and model convergence is often difficult to achieve due to the increase in non-linearity. Slatlem Vik et al. (2018) explored the THM interactions in multi-fracture plane system, demonstrating the effects of fracture spacing and thermal gradient. However, their modelling lacked a model for well flow, instead opting to divide the flow evenly between planes, and so could not account for short-circuiting phenomena studied here. Flow modelling by Asai et al. (2018) has also shown that the flow in multi-fracture doublet wells is not evenly distributed even with homogeneous fractures, highlighting the importance of a well flow model to determine the flow partitioning.

In the presence of thermoelastic effects, at reasonable circulation rates, most existing EGS models cannot realistically predict medium- to long-term behaviour. Full THM coupling is needed, coupling to well behaviour is essential, and transient effects must be addressed. In the most general case, starting from any initial configuration in which the flow is dispersed into the reservoir, the system will evolve until the vast majority of flow is concentrated along a single pathway within the reservoir. The development of short-circuiting within the system is marked by temperature breakthrough, such as observed during the long-term circulation test at the Hijori Hot Dry Rock test site (Yanagisawa et al., 2008; Tenma et al., 2008). Existing work on THM EGS models have rarely captured the general behaviour of these systems, with simulations ending before short-circuiting and the accompanying temperature breakthrough occur. The lack of temperature breakthrough is likely a consequence of the high in-situ stresses and low flow rates typically used in these models. A notable exception to this is Fu et al. (2016), who predicted temperature breakthrough accompanying the development of a short-circuit along a single dominant path within their network flow model. Fu *et al.*'s THM network flow model is two-dimensional and is unable to capture the short-circuiting phenomena studied here.

This article explores and describes the newly identified mechanisms by which short-circuiting forms in multi-fracture EGS well doublets. The general behaviour of the system is modelled, starting from the wellbore interaction with a set of initially homogeneous fractures, through to the dominance of flow along a single short-circuit pathway. A fully-coupled thermo-hydro-mechanical finite element model is developed and implemented for enhanced geothermal well systems consisting of one or more injection wells hydraulically connected to one or more production wells by one or more discrete fracture planes. One- and two-fracture EGS reservoirs with parameters based on the Utah FORGE geothermal exploration site are simulated for a period of ten years. The development

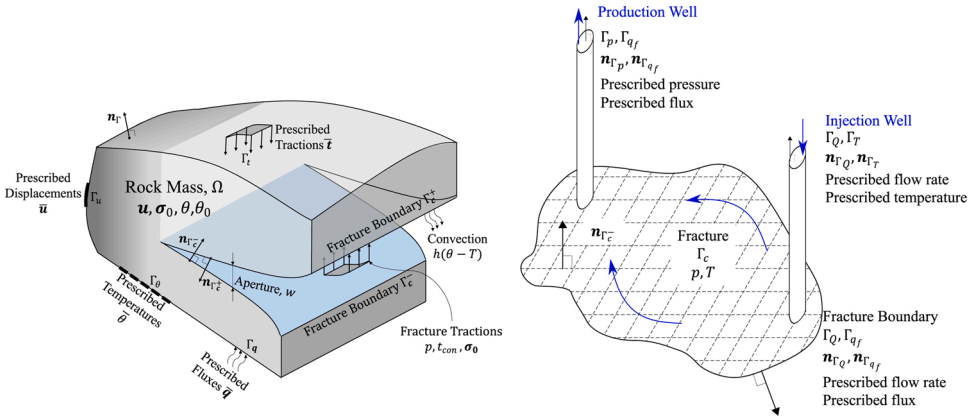

Fig. 2. Illustration of mathematical domains and boundaries. Left: solid domain, Ω, and its boundaries, $\Gamma_c, \Gamma_u, \Gamma_t, \Gamma_\theta, \Gamma_q$. Right: fluid domain, Ω_f/Γ_c, and its boundaries $\Gamma_p, \Gamma_Q, \Gamma_T, \Gamma_{q_f}$.

of multiple and complex short-circuiting phenomena are observed and described.

In the following section, a detailed description of the mathematical model, boundary conditions, and discretization is provided. Section 3 details the domain and properties of the studied well systems. In Section 4, a one-fracture EGS installation is studied to assess the behaviour of the in-plane short-circuiting mechanism known as flow channeling. The temperature response of the circulating fluid is used to identify flow regimes that correspond to particular short-circuiting developments within the system. In Section 5, a two-fracture EGS installation is studied to evaluate the development of short-circuiting in multi-fracture well systems, and identify the inter-plane short-circuiting mechanisms at the reservoir scale within multi-fracture systems. The effects of fracture spacing and well casing size are studied. Section 6 discusses the implications of short-circuiting mechanisms for naturally fractured rock masses, and Section 7 summarizes the conclusions of this study.

2. Mathematical model

This section describes the mathematical model for the enhanced geothermal system, based on the model developed and verified by Gee and Gracie (2021). The formulation is for application to a geothermal reservoir in which one or more injection wells are connected to one or more production wells by one or more fracture planes. First, the governing equations of the coupled processes are described. The governing equations are presented in non-dimensional form so that the characteristic timescale of each process may be extracted and examined. The non-dimensionalization does not limit the formulation to homogeneous, isotropic, or linear conditions. Next, the timescale of each process is considered to determine which processes may be considered transient, and which may be considered quasi-steady state (i.e., whether time-dependent terms must be considered within the governing equations). Last, the discretization and solution methods are briefly described.

2.1. Governing equations and boundary conditions

Consider a solid rock mass domain, Ω, bounded by Γ, which contains some number of discrete fractures, Γ_c, as illustrated in Fig. 2. There are four fields that exist within the domain: the solid displacement field, $\boldsymbol{u} \in \Omega$ [m], the solid temperature field, $\theta \in \Omega$ [°C], the fluid pressure field, $p \in \Gamma_c$ [Pa], and the fluid temperature field, $T \in \Gamma_c$ [°C]. In non-dimensional form, the fields are presented as

$$\boldsymbol{u}' = \frac{1}{L}\boldsymbol{u} \tag{1}$$

$$\boldsymbol{\sigma}' = \frac{1}{E}\boldsymbol{\sigma} \tag{2}$$

$$p' = \frac{p}{E} \tag{3}$$

$$\theta' = \frac{\theta - \overline{T}}{\theta_0 - \overline{T}} \tag{4}$$

$$T' = \frac{T - \overline{T}}{\theta_0 - \overline{T}} \tag{5}$$

in which the $'$ superscript denotes the dimensionless version of the corresponding field, and $\boldsymbol{\sigma}$ [Pa] is the total Cauchy stress tensor. The displacement field and coordinate systems are normalized relative to L [m], which is a characteristic length of the EGS and is assumed to the distance between the injection and production wells. Stresses and pressures are normalized relative to E [Pa], which is the elastic modulus of the rock mass. Temperatures are normalized relative to the maximum temperature difference within the system, $(\theta_0 - \overline{T})$, in which $\overline{T}$ [°C] is the temperature of the injected fluid, and θ_0 [°C] is the initial temperature of the solid rock mass.

The displacement of the rock mass, $\boldsymbol{u}'$, is governed by the equilibrium equation:

$$\frac{\beta_s}{t_u^2}\frac{\partial^2 \boldsymbol{u}'}{\partial t'^2} = \nabla \cdot \boldsymbol{\sigma}'(\boldsymbol{u}') + \beta_s \boldsymbol{g}, \quad \beta_s = \frac{L\rho_s}{E} \tag{6}$$

in which $\boldsymbol{\sigma}'$ is the dimensionless total Cauchy stress tensor, ρ_s [kg/m^3] is the density of the solid rock mass, and $\boldsymbol{g}$ [m/s^2], is the vector of acceleration due to gravity. t_u is the time scaling factor for the displacement field. The domain is assumed to be under an in-situ stress field, $\boldsymbol{\sigma}_0$, which is in equilibrium with gravity. The in-situ stress field is oriented such that the fractures are normal to the direction of the minimum in-situ stress, σ_3. Linear thermoelasticity is assumed in the rock mass such that stress and strain in the rock mass are related by the 4$^{\text{th}}$ order linear elasticity tensor, $\mathbb{C}$ [Pa]. Introducing dimensionless parameters $\boldsymbol{\sigma}_0' = \frac{1}{E}\boldsymbol{\sigma}_0$ and $\mathbb{C}' = \frac{1}{E}\mathbb{C}$, the constitutive equation relating stress and strain in the rock mass is

$$\boldsymbol{\sigma}' - \boldsymbol{\sigma}_0' = \mathbb{C}' : (\boldsymbol{\varepsilon} - \boldsymbol{\varepsilon}_\theta) \tag{7}$$

$$\boldsymbol{\varepsilon}_\theta = \alpha(\theta_0 - \overline{T})[1 - \theta']\mathrm{I} \tag{8}$$

in which $\boldsymbol{\varepsilon}_\theta$ is the thermal strain, and α [m/m°C] is the coefficient of linear thermal expansion. The linear strain tensor is defined as

$$\boldsymbol{\varepsilon} = \frac{1}{2}(\nabla \boldsymbol{u}' + \nabla \boldsymbol{u}'^{\top}) \tag{9}$$

Contact across the fractures is enforced using a penalty method. The

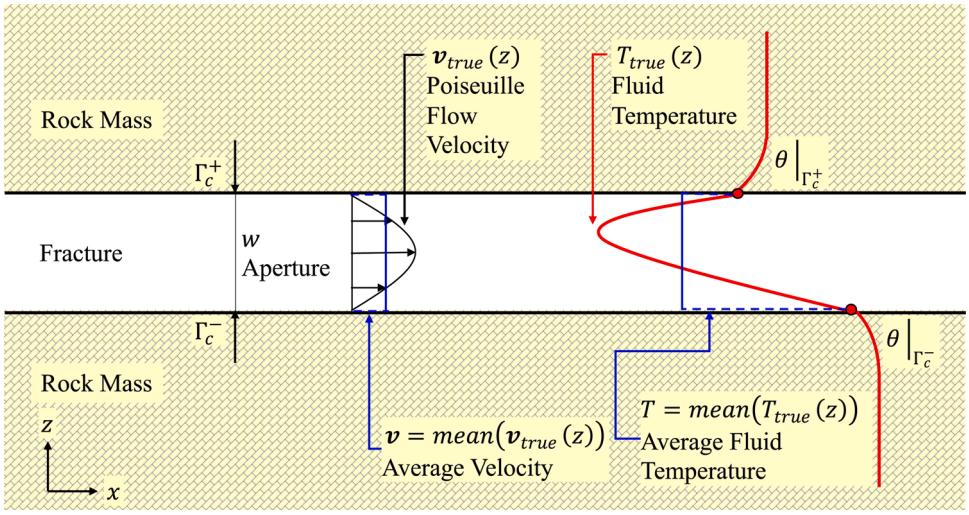

Fig. 3. Illustration of the distribution of temperature and velocity across the fracture aperture, $T_{true}(z)$ and $\boldsymbol{v}_{true}(z)$, compared with the modelled distributions, T and $\boldsymbol{v}$. T and $\boldsymbol{v}$ represent the average values of the true distributions across the aperture.

dimensionless contact traction, $\bar{t}'_{\text{con}}$, is assumed to be a linear function of the dimensionless fracture aperture, w' such that

$$\bar{t}'_{\text{con}} = \begin{cases} \dfrac{k_{\text{con}}}{E} w(\boldsymbol{u}) & \text{if } w(\boldsymbol{u}) \le 0 \\ 0 & \text{if } w(\boldsymbol{u}) > 0 \end{cases} \tag{10}$$

in which k_{con} [Pa/m] is a contact stiffness and $w(\boldsymbol{u})$ is the change in aperture due to thermo-mechanical deformation. The effective aperture of the fracture is defined as

$$w' = \frac{w}{w_0} = \frac{w_0 + w(\boldsymbol{u})}{w_0} \tag{11}$$

in which w_0 is an initial effective hydraulic aperture in the fracture. While the displacement and coordinate systems are normalized relative to L, the aperture is normalized by w_0.

The heat transfer in the rock mass is governed by conservation of energy, given by

$$\frac{L^2}{\kappa_s t_\theta} \frac{\partial \theta'}{\partial t'} = -\nabla^2 \theta' \tag{12}$$

in which κ_s [m^2/s] is the thermal diffusivity of the solid rock mass and t_θ is the time scaling factor for the solid temperature field. κ_s is defined as $\kappa_s = k_s \cdot \rho_s^{-1} \cdot c_{\text{ps}}^{-1}$, in which c_{ps} [J/kg°C] is the specific heat of the solid rock mass, and k_s [W/m°C] is the thermal conductivity of the solid domain. Heat transfer between the rock mass and fluid in the fractures is incorporated through boundary conditions acting on the internal fracture surfaces and is discussed below.

Since the rock mass is assumed to be impermeable, the fluid domain, Ω_f, is also the fracture boundary, Γ_c. In this way, the fracture planes are modelled one dimension lower than the rock mass, and thus the modelled velocity $\boldsymbol{v}'$, and fluid temperature, T', represent the average values across the fracture aperture. Fig. 3 shows the modelled averages of fluid flow and temperature within the fracture planes compared to their true distributions. The use of average fluid quantities means that, in general, a jump in the temperature field occurs between the fluid and solid at the crack surface. This is a common approach for the modelling of heat transfer in a channel (Bejan, 2013).

The fluid flow within the fractures is governed by conservation of fluid mass. The fluid is assumed to be incompressible and Newtonian. The only sources and sinks of fluid mass within the fractures are the injection and production wells. The injection and production wells are treated as point sources within the fracture. The conservation of fluid mass is given as

$$\frac{L^2 w_0}{\overline{Q} t_p} \frac{\partial w'}{\partial t'} + \nabla \cdot (\boldsymbol{q}') = q'_{\text{pi}} \delta(\text{X}_{\text{in}}) - q'_{\text{po}} \delta(\text{X}_{\text{out}}) \tag{13}$$

in which $\overline{Q}$ [m^3/s] is the prescribed fluid volume flow rate at the injection well at the surface inlet, t_p is the time scaling factor for the fluid pressure, $\boldsymbol{q}'$ is the fluid volume flux through the fracture, q'_{pi} and q'_{po} are the fluid volume fluxes from the injection and production wells respectively, and $\delta(\text{X})$ is the Dirac delta function evaluated at the inlet and outlet positions, X_{in} and X_{out}. It is assumed that there is no leakoff of fluid mass, such that all the fluid enters the domain via the injection wells and leaves via the production wells. The fracture aperture is assumed to be small such that the flow is laminar. Neglecting entrance/exit effects, the fluid flux is assumed to be given by Poiseuille flow:

$$\boldsymbol{q}' = w' \boldsymbol{v}' = \frac{w_0^3 E}{12 \mu \overline{Q}} w'^3 (\nabla p' - \beta_f \boldsymbol{g}), \quad \beta_f = \frac{L \rho_f}{E} \tag{14}$$

in which $\boldsymbol{v}'$ is the average fluid velocity, ρ_f [kg/m^3] is the density of the fluid, and μ [Pa·s] is the dynamic viscosity of the fluid.

Fracture planes are hydraulically connected to the surface and to each other by the injection and production wells, which are modelled as pipes. High flow rates are pumped through small well casings, and so large Reynold's numbers are expected within the wells. The flow is therefore governed by the Darcy-Weisbach equation. The wells are modelled as one-dimensional and any interactions with the rock mass are neglected. The conservation of mass and fluid flux within the one-dimensional wells are given as

$$0 = \frac{\partial}{\partial s'}(q'_p) \tag{15}$$

$$q'_p = \frac{\text{k E}}{L \overline{Q}} \left(\frac{\partial}{\partial s'} p' - \beta_f \boldsymbol{g} \cdot \text{n}_s \right) \quad \text{with} \quad k = \frac{\pi D^3}{2 f_D \rho_f v} \tag{16}$$

in which D [m] is the casing diameter, v [m/s] is the velocity within the well, f_D is the dimensionless Darcy friction factor, s' is the normalized local spatial coordinate along the well, and n_s is the tangent vector to the local spatial coordinate s'. The Darcy friction factor is not constant and depends on the flow regime, $f_D = f_D(\text{Re})$. For low Reynold's numbers, flow is laminar, and the friction factor can be determined analytically. For high Reynold's numbers, flow is turbulent, and the friction factor is determined from the empirical Colebrook-White equation (Colebrook,

1939). The friction factor is summarized as

$$f_D = \begin{cases} 64/\mathrm{Re} & \text{if } \mathrm{Re} < 2000 \\ \frac{1}{\sqrt{f_D}} = -2log(\frac{\epsilon}{3.7D} + \frac{2.51}{\mathrm{Re}\sqrt{f_D}}) & \text{if } \mathrm{Re} > 4000 \end{cases} \quad (17)$$

$$\mathrm{Re} = \frac{\rho_f |v| D}{\mu} \quad (18)$$

in which ϵ [m] is the pipe surface roughness. In the transitionary phase between laminar and turbulent flow, $2000 \leq \mathrm{Re} \leq 4000$, the friction factor is linearly interpolated between $f_D(\mathrm{Re} = 2000)$ and $f_D(\mathrm{Re} = 4000)$.

Heat transfer in the fluid in the fractures is governed by conservation of energy and includes contributions from heat conduction within the fluid, heat advection due to bulk motion of the fluid, and heat transfer to and from the rock mass. Following existing channel flow modelling approaches (Bejan, 2013), conservation of energy is expressed in terms of the average fluid temperature, $T^{'}$, as illustrated in Fig. 3. The fluid interacts with the rock temperature field on both sides of the fracture, Γ_c, through convection. The rate of heat transfer between the rock surface and fluid is proportional to the difference between the rock temperature at the fracture surface and the mean temperature of the fluid — i.e., it is modelled as a convective process (Bejan, 2013). These conditions appear as a boundary condition on the gradient of the rock temperature at the fracture surface, and as a body source term within conservation of energy in the fluid.

$$w^{'}\frac{\partial T^{'}}{\partial t^{'}} = -\lambda_1 \nabla\cdot(w^{'}\nabla T^{'}) + \lambda_2 \boldsymbol{q}^{'}\cdot\nabla T^{'} + \lambda_3\left[\theta^{'}|_{\Gamma_c^+} + \theta^{'}|_{\Gamma_c^-} - 2T^{'}\right] \quad (19)$$

$$\lambda_1 = \frac{\kappa_f t_T}{L^2} \quad (20)$$

$$\lambda_2 = \frac{\overline{Q} t_T}{L^2 w_0} \quad (21)$$

$$\lambda_3 = \frac{h t_T}{w_0 \rho_f c_{\mathrm{pf}}} \quad (22)$$

in which κ_f [m^2/s] is the thermal diffusivity of the fluid, t_T is the fluid temperature time scaling factor, c_{pf} [$\mathrm{J/kg^{\circ}C}$] is the heat capacity of the fluid, and h [$\mathrm{W/m^{2^{\circ}}C}$] is the heat transfer coefficient. The heat transfer coefficient governs the rate of heat transfer between the fluid and the solid, and is determined using the dimensionless Nusselt number, $\mathrm{Nu} = 2\mathrm{h}w k_f^{-1}$. This relation implies that the heat transfer coefficient is a function of the fracture aperture, $h = h(w^{-1})$. For fully developed laminar flow within a duct, the Nusselt number is a constant on the order of 10^0 (Bejan, 2013). It is assumed that the wells are insulated, such that heat transfer between the fluid and solid only occurs in the reservoir and not through the casing walls.

The boundary conditions on the solid domain are prescribed such that normal displacements on all far-field boundaries are constrained. The temperature of all far-field boundaries are fixed at the initial temperature. Three tractions act on the fracture: the in-situ stress, the fluid pressure, and the contact traction. The formal definition of the tractions on the fracture surfaces is

$$\boldsymbol{\sigma}^{'}\cdot\mathbf{n}_{\Gamma_c^{\pm}} = \left(\boldsymbol{\sigma}_0^{'} - p^{'}\mathbf{I} - \vec{t}_{\mathrm{con}}\mathbf{I}\right)\cdot\mathbf{n}_{\Gamma_c^{\pm}} \quad \text{on } \Gamma_c^{\pm} \quad (23)$$

in which $\mathrm{n}_{\Gamma_c^{\pm}}$ represent the outward facing normal of the respective fracture surface. Convection conditions, which previously appeared as a body source in the conversation of energy in the fluid, are used to define the heat flux boundary condition for the rock temperature at the fracture surface:

$$-\nabla\theta^{'}\cdot\mathrm{n}_{\Gamma_c^{\pm}} = \frac{\mathrm{hL}}{k_s}(\theta^{'}|_{\Gamma_c^{\pm}} - T^{'}) \quad \text{on } \Gamma_c^{\pm} \quad (24)$$

Table 1
Range of material properties.

Variable	Symbol	Range	Units	Reference
Rock mass mechanical parameters				
Density	ρ_s	1800–2750	kg/m^3	Somerton (1992)
Elastic modulus	E	70–140	GPa	Somerton (1992), Kolditz et al. (2012)
Poisson's ratio	ν	0.11–0.32	[–]	Somerton (1992), Kolditz et al. (2012), Heuze (1983)
Rock mass thermal parameters				
Thermal conductivity	k_s	2–4	W/m °C	Somerton (1992), Heuze (1983), Grasby et al. (2013)
Specific heat capacity	c_{ps}	800–1100	J/kg °C	Somerton (1992), Heuze (1983)
Coefficient of thermal expansion	α	8–20	× 10^{-6} m/m°C	Somerton (1992), Heuze (1983)
Fluid mechanical parameters				
Density	ρ_f	950–1100	kg/m^3	Walsh et al. (2017)
Viscosity	μ	0.2–1.4	mPa· s	Walsh et al. (2017)
Fluid thermal parameters				
Thermal conductivity	k_f	0.6–0.7	W/m°C	Walsh et al. (2017)
Specific heat capacity	c_{pf}	3500–5000	J/kg °C	Walsh et al. (2017)
Nusselt number	Nu	1–9	[–]	Bejan (2013)

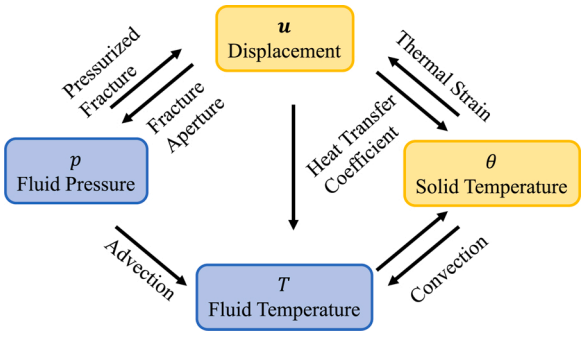

Fig. 4. Representation of the interconnectivity between fields and the methods through which they are coupled.

At the injection well, flow rate and injection temperature, $\overline{Q}$ and $\overline{T}$, are prescribed. At the production well, pressure is prescribed at atmospheric pressure. Around the edges of the fractures, fluid flow is restricted such that there is no fluid leakoff through the edges of the fluid domain. At both the edges of the fractures and the production well, the conductive heat flux is restricted such that no energy may leave the domain by conductive heat flux. However, this boundary condition does not prevent energy from leaving the domain through advective heat flux. As fluid flow is restricted around the edges of the fracture, there is neither conductive nor advective heat flux out of the domain through the edges of the fracture. An advective flux exists only at the production well, such that energy within the system may only leave the system via advection out of the production well.

The range of all of the material parameters is shown in Table 1 for a low permeability rock mass such as granite, and water as the working liquid. Some material parameters, such as viscosity, are highly dependent on pressure and temperature. For this model, all material properties are treated as homogenous, isotropic constants such that the nonlinearity of the system is strictly a result of the coupling between fields. In this way, the model includes only the minimum number of sources of

complexity for the coupled system so that the study of short-circuiting mechanisms could be separated from other phenomena resulting from nonlinear, heterogeneous, or anisotropic conditions. The coupling between the fields is illustrated in Fig. 4, which shows that there is a high degree of interconnectivity and dependence between the fields.

2.2. Characteristic timescales

In this section, the characteristic timescale of each process within the system is considered to determine an order of magnitude approximation. The characteristic timescales will indicate which fields have transient effects that dissipate quickly relative to the timespan of interest, and therefore which processes may be considered as quasi-steady state and which must be considered as transient. A simplified one-dimensional geometry is considered with a single injection and production well and a single crack plane.

By considering the range of the timescales for processes in an EGS, it will be demonstrated that a disparity exists between the rate of heat transfer in the rock mass and all other processes. Heat transfer in the rock mass is slow, while heat transfer and pressure diffusion in the fluid are fast processes. While it is common to model the rock mass as quasi-static, it is also common to model both heat transfer in the fluid and pressure diffusion through the fracture as transient processes, e.g., Guo et al., 2016; Slatlem Vik et al., 2018. The disparity in timescales shows that the rock temperature is the only field that must be considered transient, and the model can gain efficiency by assuming the heat transfer and pressure diffusion in the fracture are quasi-steady state. Quasi-steady state does not imply that these processes do not change over time, but rather that the time-dependent terms within the governing equations may be neglected.

First, consider the temperature in the rock mass. The conservation of energy for both the rock and fluid are parabolic partial differential equations (PDEs), as is the conservation of fluid mass. Once perturbed, these processes will tend towards a steady-state solution over time in an exponential manner. In general for parabolic PDEs, the characteristic timescale is given by the time scaling coefficient, such that the characteristic timescale emerges naturally from the normalization of the PDE. The characteristic timescale of the rock temperature, t_θ, is thus given by

$$t_\theta = \frac{L^2}{\kappa_s} \tag{25}$$

in which L [m] is a characteristic length for the solid temperature field. The length scale for the solid domain is not well-defined, as ideally the solid domain is semi-infinite in the out-of-plane direction. The characteristic length of the solid domain is therefore assumed to be the distance between the injection and production wells. The distance between wells is a design parameter unique to each installation. For the purpose of estimating the characteristic timescales, a range of $100 \leq L \leq 2000$ m is adopted. Combined with the range of thermal properties from Table 1, the characteristic time for the solid temperature field is $100 \leq t_\theta \leq 2 \times 10^5$ years.

Next, consider the displacement field. The equilibrium equation is a hyperbolic PDE, so the system will never return to rest without the introduction of damping, and therefore the characteristic timescale does not emerge naturally from the PDE. In an EGS, large amounts of damping are provided by the fluid and the fractured rock mass. It is therefore assumed that the time required for the system to come to rest after perturbation is on the same order of magnitude as wave propagation through the rock mass. The characteristic timescale, t_u, is thus found from the elastic wave speed equation and the displacement field time scaling factor such that

$$t_u = L\sqrt{\frac{\rho_s}{E}} \tag{26}$$

in which L [m] is a characteristic length for the displacement field. L is again assumed to be at least the distance between the injection and production wells, $100 \leq L \leq 2000$ m. Combined with the range of mechanical properties from Table 1, the characteristic time for the displacement field is $10 \leq t_u \leq 390$ ms.

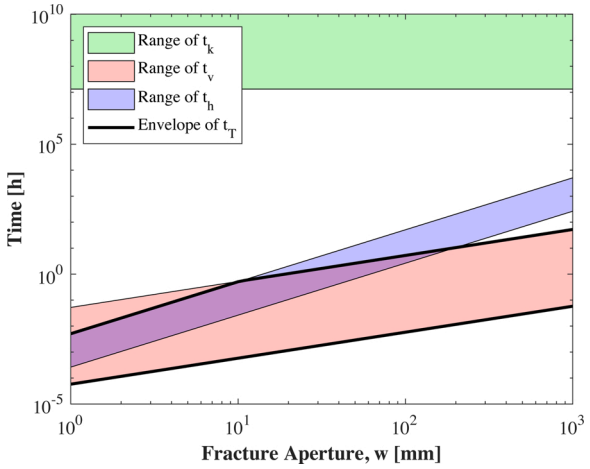

Fig. 5. Range of competing timescales within the fluid temperature. In general, advection is the dominant process within the fluid temperature, though at low flow rates and low apertures conduction may be dominant.

Next, consider the conversation of mass for the fluid. Following a methodology similar to Pierce (Peirce and Detournay, 2008), Eqs. (13) and (14) can be non-dimensionalized to remove w_0, which is generally unknown and difficult to estimate. The characteristic timescale, t_p, is therefore

$$t_p = \frac{L^2}{\overline{Q}}\left(\frac{12\mu\overline{Q}}{E}\right)^{\frac{1}{3}} \tag{27}$$

in which L is a characteristic length for the fluid pressure field. $\overline{Q}$ is a prescribed boundary condition, but is expected to fall within the range of $10 \leq \overline{Q} \leq 150$ L/s under operating conditions for an economically viable well (Xie et al., 2015). Combined with the range of fluid properties from Table 1, the characteristic time for the pressure field is $0.2\,\text{s} \leq t_p \leq 2\,\text{h}$.

Last, consider the temperature within the fluid. There are three competing timescales in this equation: one for conduction t_k, one for advection t_v, and one for convection t_h. The governing timescale within the fluid temperature is always the fastest of the competing timescales. The characteristic timescale of heat transfer in the fluid is summarized as

$$t_T = min\begin{cases} t_k = \dfrac{L^2}{\kappa_f} \\ t_v = \dfrac{L}{\overrightarrow{v}} \\ t_h = \dfrac{\rho_f c_{pf} w}{h} = \dfrac{2w^2}{\text{Nu}\cdot\kappa_f} \end{cases} \tag{28}$$

in which $\overrightarrow{v}$ is the fluid velocity, and L is a characteristic length. Let the fluid velocity be estimated as the average velocity leaving the well

$$\overrightarrow{v} = \frac{\overline{Q}}{\pi \text{D w}} \tag{29}$$

in which D is the diameter of the injection well casing, and w is the fracture aperture. A typical geothermal well casing will have a diameter in the range of $10 \leq D \leq 30$ cm (Grasby et al., 2013). t_k and t_v are both functions of L, the in-plane characteristic length scale which is a property of the geometry and does not change during the simulation. However t_v and t_h are both functions of w, the fracture aperture, which

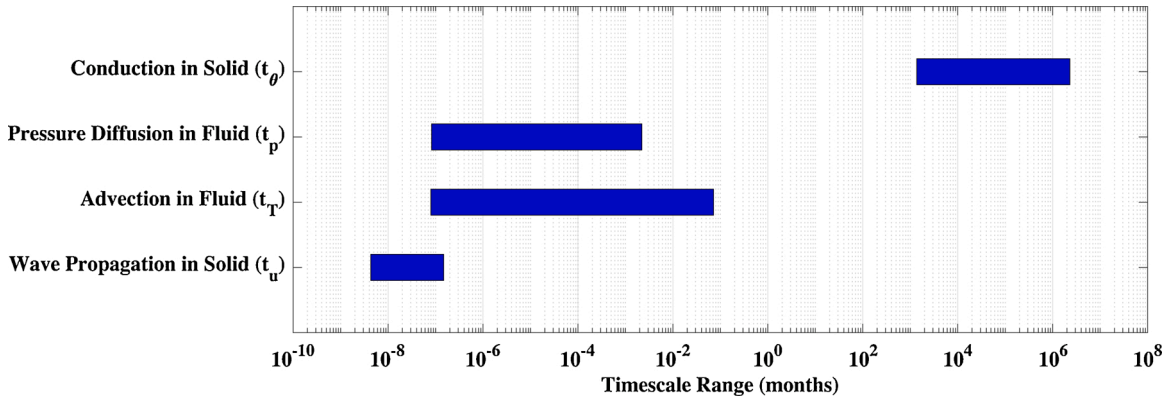

Fig. 6. Range of timescales for all physical processes within the system. The rate of heat conduction within the solid rock mass is at least four orders of magnitude slower than all the other processes.

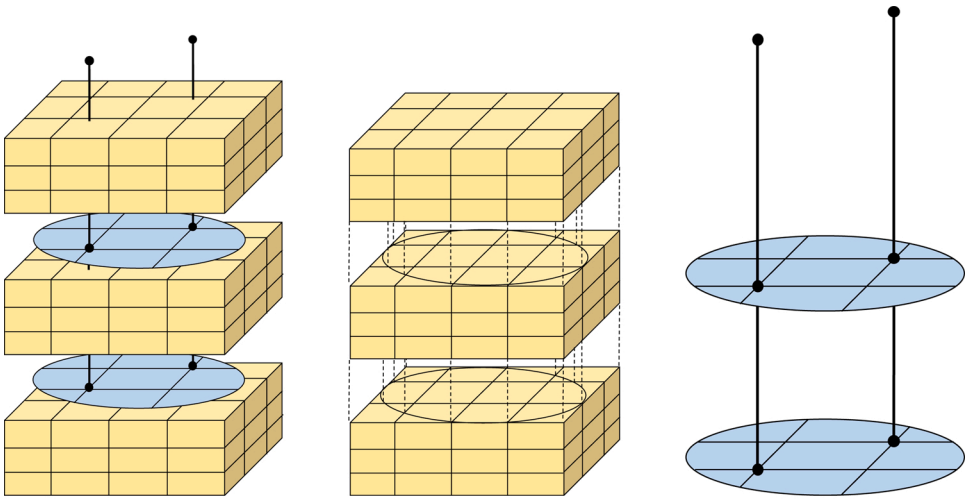

Fig. 7. Assembly of the EGS finite element model using three-dimensional rock masses, two-dimensional fracture planes, and one-dimensional wells. Figure (a) shows the complete assembly of the model. Figure (b) shows the solid domain blocks, which are connected to each through shared nodes beyond the fracture boundary. Fig. (c) shows the fluid domain, which comprises of two-dimensional fracture planes and one-dimensional wells. The fracture planes are connected to each other and the surface through the wells. The wells pass through the rock mass blocks, but do not interact with them.

increases over time. The range of fracture apertures is difficult to estimate without simulating the entire system, so a large range is adopted to show that the timescale is small regardless. The range of timescales as a function of aperture and the corresponding envelope of the overall fluid temperature timescale are shown in Fig. 5. In general, advection is the dominant process governing the fluid temperature, but convection may be dominant at low apertures. Conduction in the fluid is very slow, and practically negligible compared to advection, indicating Pe >> 1. The overall timescale envelope for characteristic timescale in the fluid is $0.2\,\mathrm{s} \leq t_T \leq 50\,\mathrm{h}$.

The timescales for the transient behaviour of all four fields are shown in Fig. 6. The characteristic timescales can be summarized as follows: inertial effects within the displacement field occur on the order of milliseconds, transient effects within the fluid pressure and temperature occur on the order of hours, and transient effects within the rock temperature occur on the order of years. The characteristic timescales of the fluid processes can be scaled for different design conditions such as the number of independent crack planes or multiple outlet wells. Regardless, the difference in timescales between the fields is so large that the displacement, pressure, and fluid temperature may be considered quasi-steady state. Assuming that the processes are quasi-steady state does not imply that they do not change over time, but rather that transient effects dissipate quickly relative to the timescale of interest and therefore some time-dependent terms which appear in the governing equations can be omitted as their contributions to the system response will be negligible. Only when considering very short time periods do the transient effects of these fields need to be considered. Therefore, for analyses concerned with the long-term behaviour of enhanced geothermal systems, only heat transfer in the rock mass needs to be considered as transient.

2.3. Discretization and solution method

The governing equations are discretized and approximately solved using the finite element method. Three dimensional eight-node brick elements are used for the solid domain, two dimensional four-node bilinear elements are used for the fluid domain, and one dimensional two-node linear elements are used for the wells. Fig. 7 shows the assembly of the model.

A backwards Euler method of time integration is used to mitigate the development of spurious oscillations in the solid temperature field (Harari, 2004; Faragó and Horváth, 2007). The Streamline-Upwind-Petrov-Galerkin (SUPG) method is applied to the heat transfer in the fluid to prevent the spurious osicllations due to advection dominant flow in the fluid temperature (Brooks and Hughes, 1982). The set of coupled discrete equations is solved using a fully-coupled Newton-Raphson iterative scheme. Aitken's Δ^2 relaxation method is introduced to the Newton-Raphson scheme to increase robustness of the solution (Küttler and Wall, 2008).

A comprehensive description of the discretization and verification of the numerical solution scheme is provided in Gee and Gracie (2021).

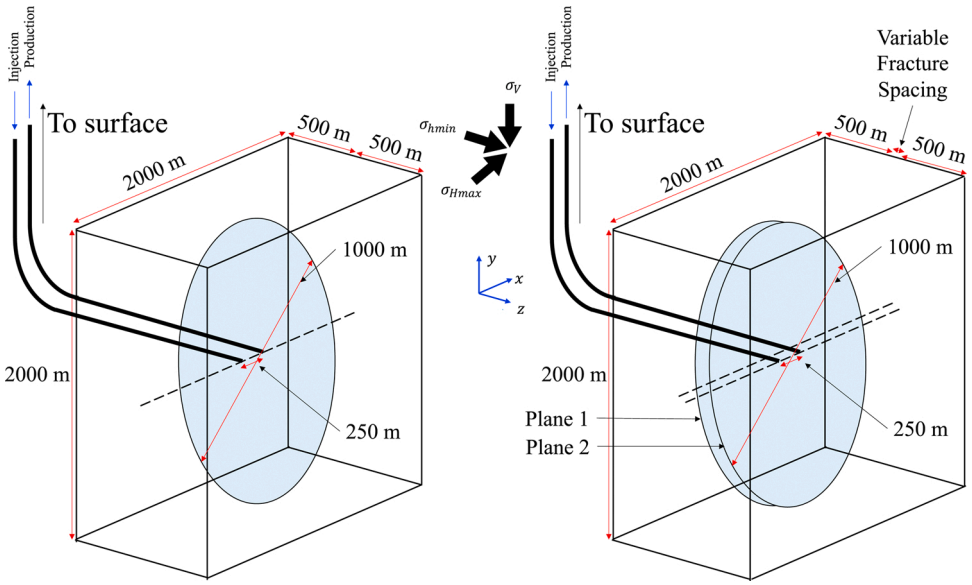

Fig. 8. Computational domains for the sample problems with vertical fractures (not to scale). Left: domain for the one-fracture system. Right: domain for the two-fracture system. The fracture planes are aligned along the *XY* plane, such that the *Y*-axis is vertical.

Table 2
Material parameters and boundary conditions for sample problems.

Parameters	Variable	Units	Sample wells
Rock mass density	ρ_s	kg/m^3	2750
Rock matrix elastic modulus	E	GPa	59
Rock matrix Poisson's ratio	ν	[–]	0.28
Rock mass thermal conductivity	k_s	W/m °C	3.05
Rock mass heat capacity	c_{ps}	J/kg °C	790
Coefficient of thermal expansion	α	$\times 10^{-6}$ m/m °C	8
Fluid density	ρ_f	kg/m^3	1000
Viscosity	μ	mPa · s	1
Fluid thermal conductivity	k_s	W/m °C	0.6
Fluid heat capacity	c_{pf}	J/kg °C	4200
Nusselt number	Nu	[-]	5
Injection rate	$\overline{Q}$	L/s	50
Outlet pressure	$\overline{p}$	kPa	100
Well casing diameter	D	cm	22
Pipe surface roughness	ϵ	mm	0.25
Depth	L_P	m	1800
Initial fracture hydraulic aperture	w_0	mm	3
In-situ stress	σ_V	MPa	39
	σ_{Hmax}	MPa	31
	σ_{hmin}	MPa	26
Initial reservoir temperature	θ_0	°C	225
Injection temperature	$\overline{T}$	°C	70

3. Description of simulated wells

This section describes the geometry, in-situ conditions, and simulation parameters of the well systems considered in the following sections.

An EGS well doublet is considered where the injection and production wells are hydraulically connected by fracture planes. The wells are horizontal and at the same elevation. The fracture planes are aligned vertically and normal to the direction of the minimum in-situ stress. A constant hydrostatic pressure is assumed within the fracture, and as the fluid phase is water, gravity-induced advective effects are small and are ignored.

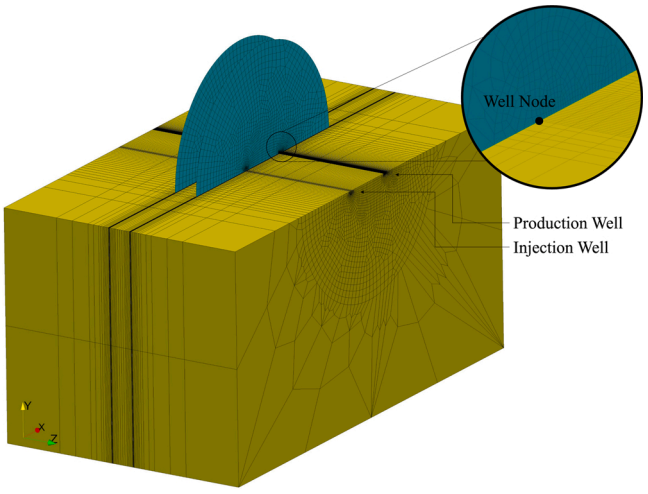

Fig. 9. Illustration of the unstructured mesh for the two-fracture EGS model. Symmetry of the system is used along the plane that is aligned with the wells and normal to the fractures.

The injection and production wells are spaced 250 m apart at a mean depth of 1800 m, as shown in Fig. 8. The simulated domain is 4 km^2 by 1 km. The fractures are assumed to be planar and circular with a diameter of 1000 m. On the exterior faces of the solid domain, normal displacements are constrained and the temperature is fixed at the initial temperature of 225 °C. The boundaries of the domain are placed far enough away from the fractures that they have no impact on the behaviour of the system. The initial temperature and the in-situ stresses are assumed to be uniform. The parameters and in-situ conditions are based on the Utah FORGE enhanced geothermal testing site, listed in Table 2 (U.S. D. of Energy, 2020). The simulated rock mass is assumed to be homogenous and so the mean values of the FORGE site parameters are used. The only deviation from the FORGE dataset is that the coefficient of thermal expansion, α, has been increased from 2×10^{-6} m/m °C to 8×10^{-6} m/m °C, as the original value was deemed too low for a granitoid rock mass.

In the simulation, 70 °C water is injected at 50 L/s for 10 years. The injection rate is linearly ramped-up over the first four months, then kept

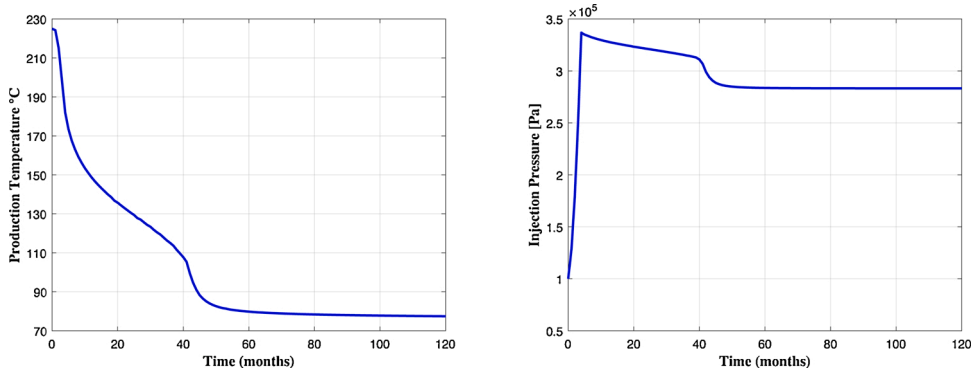

Fig. 10. Production temperature and surface injection pressure for a single fracture EGS. Production temperature is the temperature of the working fluid from the production well at the surface. The total pressure within the fracture is higher than the injection pressure at the surface due to the hydrostatic pressure provided by the well depth.

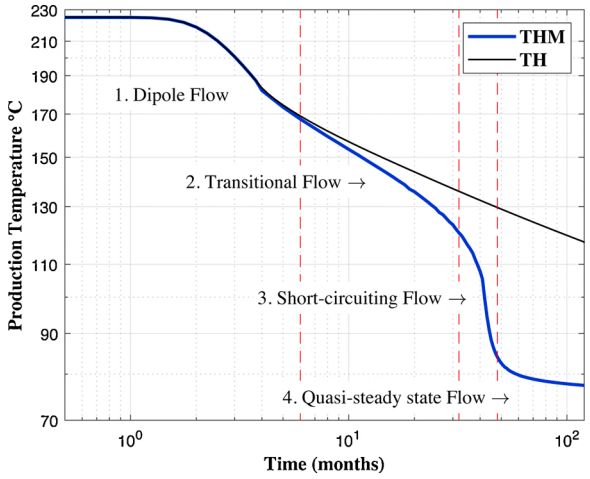

Fig. 11. Production temperature from a single fracture EGS, plotted on a log-log scale. Four production regimes are identified, corresponding to different behaviours within the fracture. THM represents the results of the coupled thermo-hydro-mechanical model, while TH represents the results of a hydro-thermal model in which mechanical deformation is neglected.

constant. Timesteps of 0.5 months were used for the first 2 years, and 1 month timesteps thereafter. The meshes used for the fluid and solid domains are illustrated in Fig. 9. A coarse mesh is used around the edges of the domain while a fine mesh is used around the injection and production wells. There are 2172 fluid elements in each fracture plane. The smallest elements have a characteristic length of 0.25 m. The fluid and solid meshes are conforming so there is an exact correspondence between the nodes and element faces of the solid and fluid meshes.

4. In-plane short-circuiting mechanisms

In this section, the in-plane short-circuiting mechanism of the single fracture plane EGS is identified and discussed. The behaviour of the system has four production regimes which correspond to specific multi-physics processes within the reservoir.

Fig. 10 illustrates the production temperature and injection pressure of the single fracture plane EGS. Fig. 11 shows the temperature at the production well plotted on a log-log scale. The logarithmic scale highlights the decaying exponential nature of the production curve and allows for the identification of four distinct phases of production: (1) dipole flow; (2) transitional flow; (3) short-circuiting flow; and (4) quasi-steady state flow. Fig. 12 shows the fluid temperature, fracture aperture, and fluid velocity within the fracture for the single fracture EGS at four points in time, each illustrating one of the four stages of production. The contour plots of temperature and aperture within the dipole and transitional regimes show qualitative agreement with previously published work (Guo et al., 2016; Salimzadeh et al., 2018b; Slatlem Vik et al., 2018).

Dipole flow is the first flow regime that develops within the fracture plane. Thermo-mechanical deformation is not significant during this first phase, and so the production temperature is nearly identical to that of a TH model which neglects deformation. Hot fluid flows into the production well from all sides and the flow near the production well is a mirror image of the flow around injection well. The flow pattern within the fracture plane is similar to a dipole pattern in an electromagnetic field, hence the name dipole flow. This production regime is short-lived.

Transitional flow is the second flow regime and develops after 6 months for this scenario. The aperture increases near the production well, creating a bias for the production well to accept flow from the direction of the injection well (Fig. 13a). The fluid velocity contours shift away from a dipole pattern, as the velocity on the far side of the production well decreases. The rate of production temperature decrease is greater than the TH model, demonstrating how any model which neglects mechanical deformation is over-optimistic about the potential of an EGS installation. A secondary area of increased aperture, apparent in Fig. 13b, develops around the injection well, slowing the velocity leaving the injection well. Both areas of aperture growth contribute to the development of short-circuiting, but there are different mechanisms at work driving the fracture opening. Around the injection well, the cooling and contraction are locally axisymmetric. Aperture growth in this area is therefore a largely thermal effect as thermal strain overcomes the effective in-situ stress which keeps the fracture closed. Around the production well, there is a sharp thermal front — the rock mass on the injection side of the well is cool but the rock mass on the far side remains hot. Non-uniform cooling at the production well induces rotational deformation of the rock mass and drives the development of aperture growth in this area. The different aperture growth mechanisms are evidenced by the difference in the stresses around the wells, as illustrated in Fig. 14. The stress state around the injection well is simple; normal stress is approximately uniform, and shear stress is low. The stress state around the production well is complex, as the sharp thermal front creates large shear stresses and high normal stress gradients. Aperture growth around the production well is largely a mechanical effect from the deformation of the sharp thermal front and is further explained through the use of a two-dimensional analogous situation in Appendix A. In this specific case, the aperture around the production well is much larger than around the injection well, but this is not true for all systems as it is dependent on the mechanical and thermal parameters and in-situ conditions of the rock mass. At both the injection and production wells, the aperture growth mechanisms are driven by thermo-elastic effects rather than the effects of fluid pressure.

After 32 months, short-circuiting flow develops within the fracture.

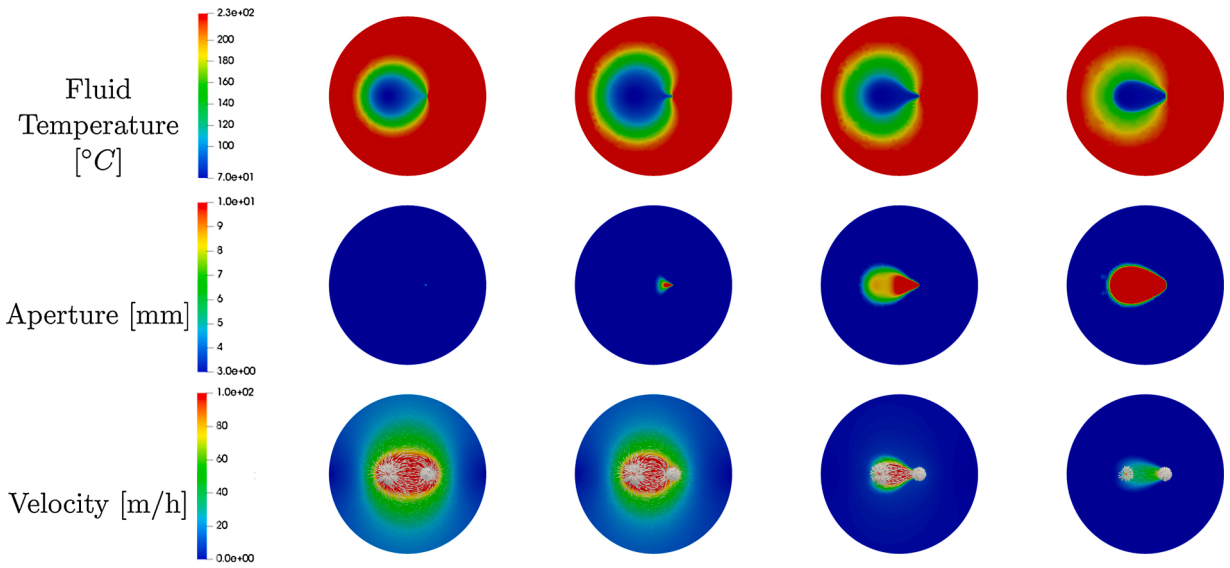

Fig. 12. Development of flow channeling in a single fracture EGS. Fluid temperature, fracture aperture, and fluid velocity are plotted over time. The injection well is located on the left of each image and the production well is located on the right. Images are taken at 6 months, 32 months, 48 months, and 90 months which fall within the dipole, transitional, short-circuiting, and quasi-state steady production regimes respectively.

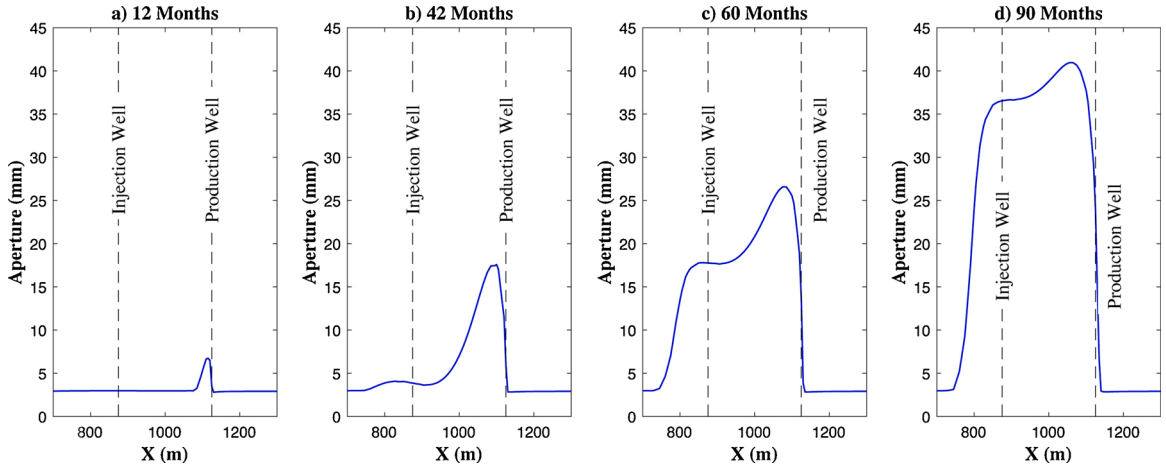

Fig. 13. Aperture along the fracture centerline of a single fracture EGS. 12 months corresponds to the transitional flow regime, in which the aperture change begins to affect the flow pattern. 42 months corresponds to the short-circuiting flow regime, in which two separate areas of increased aperture around the injection and production wells link together a channel with decreased flow resistance. 60 and 90 months correspond to the quasi-steady state regime, in which the channel is open and aperture continues to grow over time, restricting flow to a decreasing area.

This production regime is marked by a drastic temperature breakthrough in which there is a large decrease in the outlet temperature in a short period of time. The cause of this behaviour is flow channeling – a positive feedback loop that begins to develop in the transitional regime. Short-circuiting is marked by the union of the two regions of increased aperture around the injection and production wells, forming a single open channel within the fracture plane. This open channel allows the fluid to flow out of the injection well and directly towards the production well, bypassing the hotter rock regions. The observed temperature breakthrough during this phase echoes the results of Fu et al. (2016).

Short-circuiting flow is relatively short-lived, and the production quickly decays into a quasi-steady state regime by 48 months. The quasi-steady state regime is so named because there is little change in the production temperature or the inlet pressure, such that from the perspective of an operator the only two quantities that can be directly and continuously measured are in a steady-state condition. The fracture aperture slowly continues to increase and the fluid flux follows the aperture contours, becoming restricted to the channel and increasing over time. While the fluid flux increases in the channel, the fluid velocity within the channel decreases over time. As the cold injected fluid is confined to the channel, increased heat recovery occurs from the far side of the injection well, accompanied by a small recovery in the fracture aperture. Quasi-steady state flow is a stable configuration for the system — disrupting the open channel configuration will require a change to the pumping operations, such as pumping to a new production well, injecting heat, or allowing heat recovery.

5. Multi-fracture short-circuiting mechanisms

Increasing the number of fracture planes is a tempting method to increase the productivity of the EGS. Flow is initially distributed between the fracture planes, increasing the active area over which heat transfer occurs and raising the temperature at the production well. However, multi-fracture EGSs exhibit increased thermo-mechanical and hydro-mechanical interaction which appear to compromise the viability of simply operated multi-fracture EGSs. In this section, the influence of

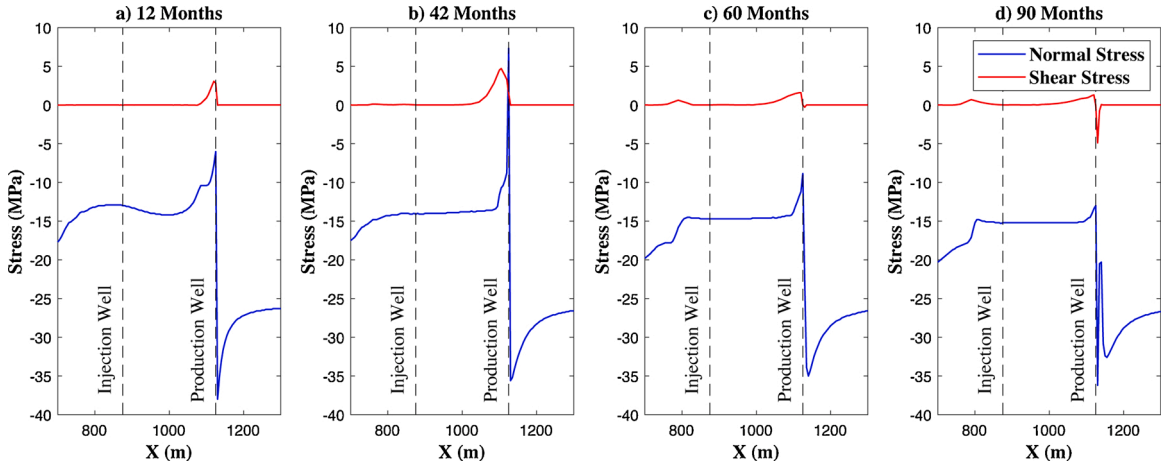

Fig. 14. Stress along the fracture surface centerline of a single fracture EGS. Normal stress, σ_{zz}, is the total stress normal to the fracture along the fracture centerline. Shear stress, σ_{xz}, is the total stress component along the plane normal to the fracture and aligned with the wells. Shear stress around the production well in the early phases indicates that aperture growth around the production well is the result of rotational movement of the rock mass due to the sharp thermal front.

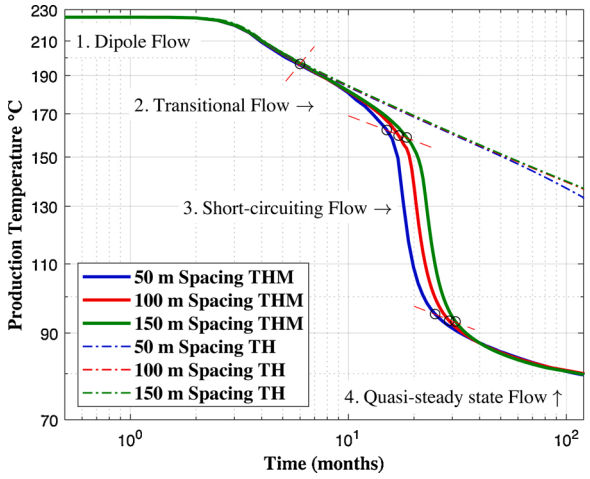

Fig. 15. Flow regimes for a two fracture EGS with variable spacing. The onset of the short-circuiting regime is defined as the point when the rate of heat decrease exceeds − 4 °C per month, and the onset of the quasi-steady state regime is defined as the point when the rate of heat decrease is less than − 1 °C per month.

two variables, fracture spacing and well casing diameter, are examined. The systems studied demonstrate inter-plane short-circuiting mechanisms, in addition to more complex in-plane short-circuiting mechanisms.

5.1. Fracture spacing and thermo-elastic interaction

Fig. 15 shows the production temperature for a two-fracture EGS where the fractures are spaced at 50, 100, and 150 m. The four production regimes are identified. The onset of short-circuiting flow is defined as the point at which the rate of production temperature decrease exceeds − 4 °C/month, and the onset of the quasi-steady state regime is defined as the point when the rate of heat decrease is less than − 1 °C/month. These threshold values are only applicable to this system with the specified flow rate. With these definitions, there is a power-law relationship between the production phase timing and the fracture spacing, given by

$$t_{SC} = 7S^{0.19} \tag{30}$$

$$t_{QSS} = 11.5S^{0.20} \tag{31}$$

in which S [m] is the fracture spacing, t_{SC} [months] is the time to the onset of the short-circuiting regime, and t_{QSS} [months] is the time to the

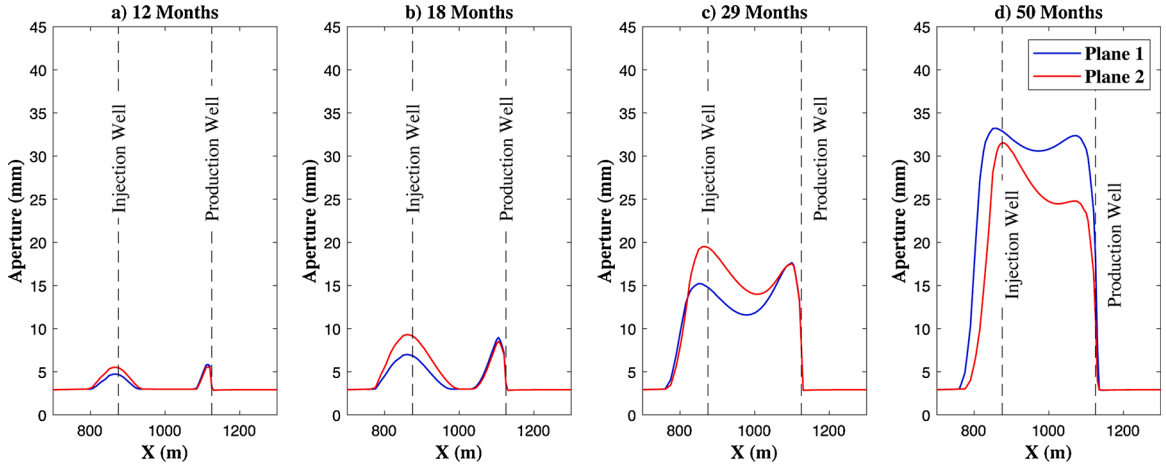

Fig. 16. Aperture along the crack centerline during different production phases in the two-fracture EGS with 100 m spacing. 12 months corresponds to the transitional flow regime. 18 months corresponds to the short-circuiting flow regime. 60 and 90 months correspond to the quasi-steady state regime. Apertures around the injection well are much higher than the one-fracture EGS due to increased thermal contraction in the rock mass between planes.

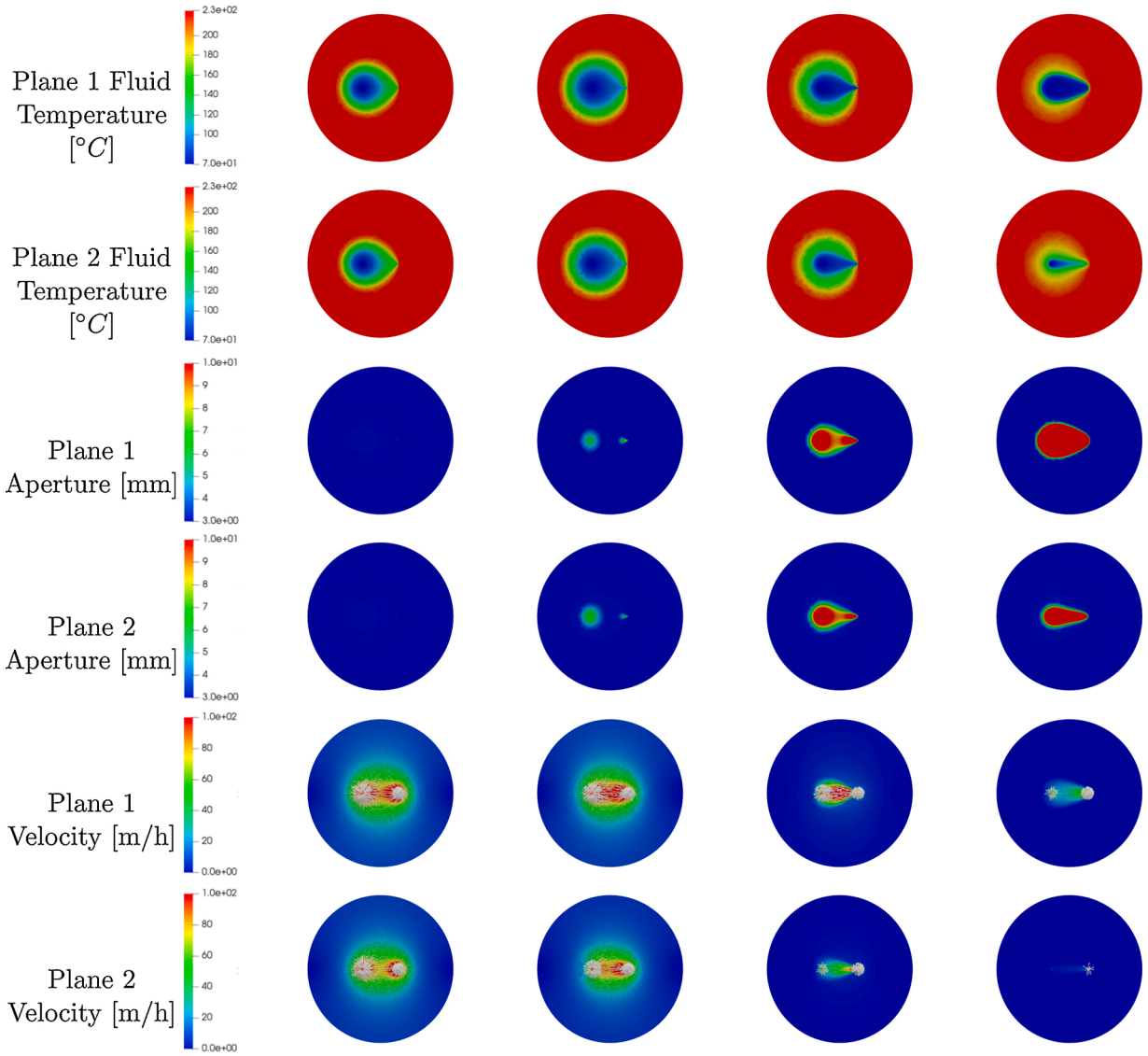

Fig. 17. Development of flow channeling within a two-fracture EGS with 22 cm wells and 100 m spacing between fracture planes. Fluid temperature, fracture aperture and fluid velocity are plotted. The injection well is located on the left of each image and the production well is located on the right. Images are taken at 6 months, 18 months, 29 months, and 90 months which fall within the dipole, transitional, short-circuiting, and quasi-state steady production regimes respectively.

onset of the quasi-steady state regime. The similar exponents in Eqs. (30) and (31) indicate that fracture spacing has little impact on the duration of the short-circuiting regime.

The production temperature of the two-fracture EGS is initially much higher than the single fracture EGS. Transitional flow begins at roughly the same time as the one-fracture EGS. Short-circuiting occurs between 17–20 months, which is sooner than the 32 months observed in the single fracture EGS. The reason for this disparity is the increased amount of thermal contraction occurring within the rock mass. The rock mass sandwiched between the two fractures experiences heat loss on both sides, resulting in increased contraction, which creates higher apertures within the fracture planes, which in turn causes short-circuiting to develop sooner. The higher apertures are illustrated in Fig. 16. The development of the fluid temperature, aperture, and velocity profiles

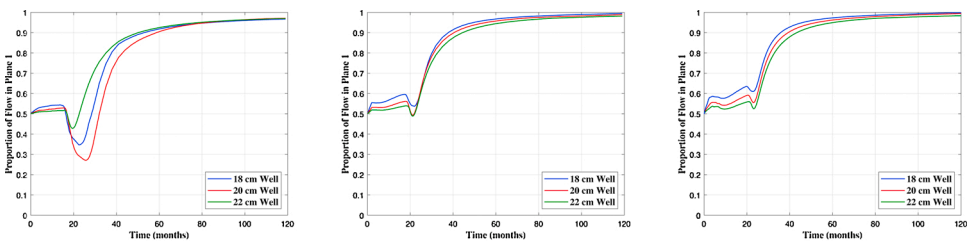

(a) 50 m Spacing (b) 100 m Spacing (c) 150 m Spacing

Fig. 18. Proportion of flow in Plane 1 for 50, 100, and 150 m fracture spacing and well casing diameters of 18, 20, 22 cm. In all cases, the two-plane flow decays to flow in Plane 1 only.

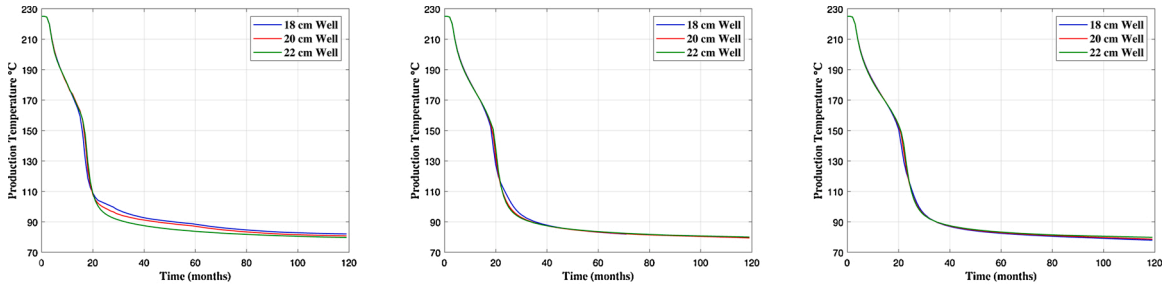

(a) 50 m Spacing (b) 100 m Spacing (c) 150 m Spacing

Fig. 19. Production temperature of multi-fracture wells with different fracture spacing and well casing diameters. While well casing size can greatly affect the flow distribution in the reservoir, these differences are not reflected in the production temperature.

within the two-fracture EGS are illustrated in Fig. 17.

5.2. *Plane channeling – reservoir scale short-circuiting*

Fig. 17 illustrates both in-plane and inter-plane short-circuiting mechanisms that arise in multi-fracture EGS. Plane channeling is a reservoir scale inter-plane short-circuiting mechanism in which the multi-plane flow devolves to single plane flow. Plane channeling only manifests when considering an interconnected fracture and well flow model. Plane channeling forms a positive feedback loop with flow channeling, as increased flow through a single plane exacerbates the development of flow channeling, which leads to more flow through that plane.

Plane channeling is induced by the friction head loss in the wells between fractures. Although the initial hydraulic conductivity of the two fractures is identical, the addition of well casings creates an asymmetric system, and this perturbation leads to the development of plane channeling. The partitioning of flow between planes for fracture spacings of 50 m, 100 m, and 150 m is illustrated in Fig. 18. Flow partition curves are shown for well diameters of 18 cm, 20 cm, and 22 cm. While the casing diameters can have large effects on the behaviour of flow within the reservoir, these changes are not reflected in the production temperature, as demonstrated in Fig. 19. Therefore, in this system, the production temperature of the system is dominated by the in-plane short-circuiting mechanism.

Reducing the casing diameter encourages flow through Plane 1, and it is observed that the initial flow partition always favours Plane 1. Despite this, flow channeling occurs in Plane 2 before Plane 1 in all

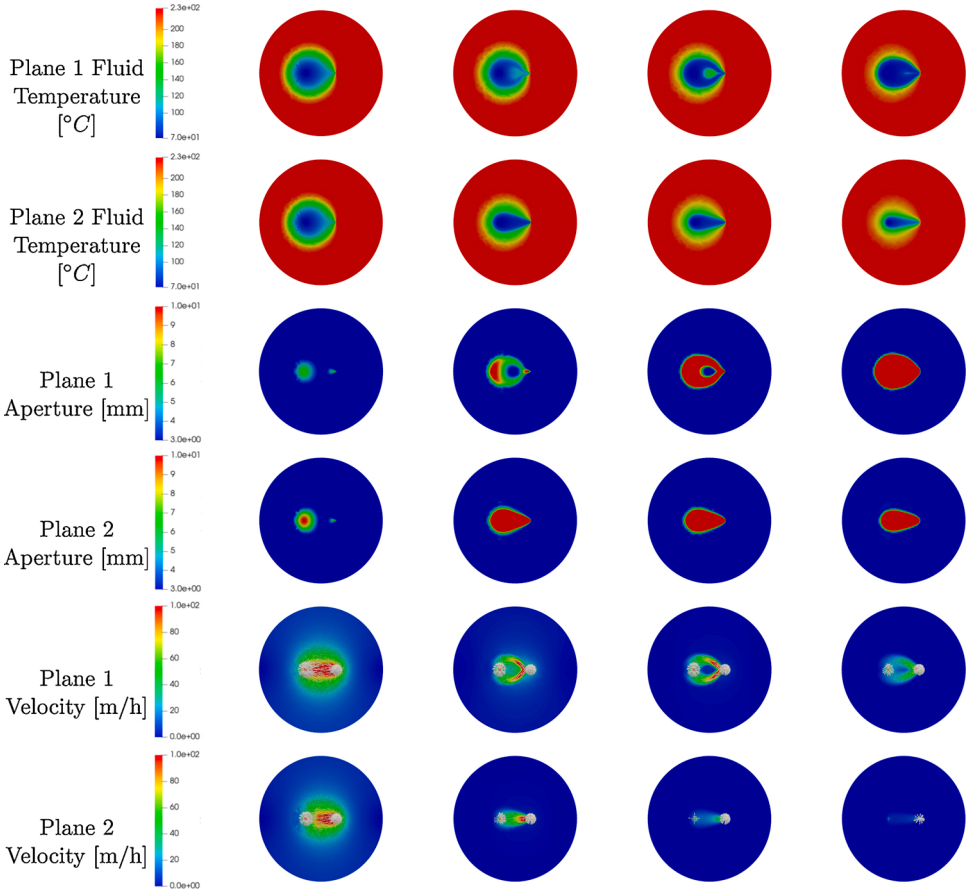

Fig. 20. Bifucation of the short-circuiting pathway in a two-fracture EGS with 20 cm well casings and 50 m fracture spacing. Fluid temperature, fracture aperture and fluid velocity are plotted. The injection well is located on the left of each image and the production well is located on the right. Images are taken at 15 months, 25 months, 35 months, and 60 months. The fluid in Plane 1 must reroute around the area of decreased aperture created by hydro-mechanical interaction with Plane 2.

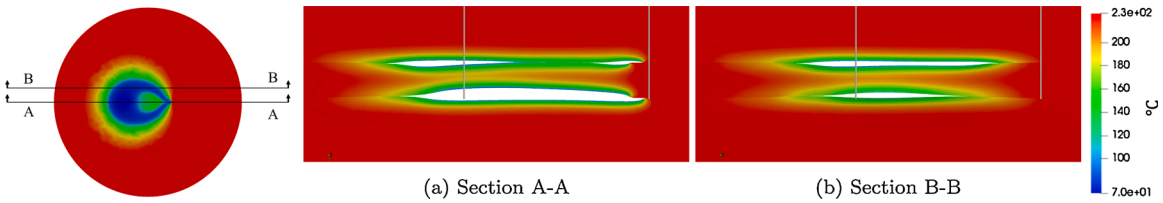

Fig. 21. Deformed shape of the rock mass at sections for the alternative short-circuiting path case at 35 months. The rock temperature is shown with displacements amplified × 500. The pressure in Plane 2 closes Plane 1 along the midline, causing the development of an alternative short-circuiting path in Plane 1. Section A-A cuts along the midline between the wells. Section B-B is offset 75 m from the midline and does not cut through the wells, but the well positions are shown for reference. The injection and production wells are shown in their positions in the undeformed configuration.

cases, reflected by a decrease in the proportion of flow through Plane 1 at the onset of the short-circuiting regime. This is due to the higher average fluid pressure within Plane 2. The pressure drop across Plane 1 must be equal to the pressure drop across Plane 2 plus the pressure drop in the connecting wells. Therefore, the pressure drop across Plane 2 is smaller than the pressure drop across Plane 1, resulting in a higher average fluid pressure within Plane 2 that causes initially larger apertures. The higher apertures in Plane 2 are reflected in Fig. 16.

Although in-plane short-circuiting occurs in Plane 2 before Plane 1, it does not become the dominant flow plane. The additional resistance offered by the well casings results in a strong preference for Plane 1 to become the dominant plane. In all tested cases, in-plane short-circuiting occurs in Plane 1 not long after Plane 2, and the flow decays to single-plane flow through Plane 1 over time. An exception to this behaviour is observed in the 50 m spacing with 18 and 20 cm well casings, in which Plane 2 dominant flow persists much longer than all other cases. In these cases, plane channeling interacts with flow channeling to create alternative (bifurcating) short-circuiting pathways not previously observed, discussed in the following section.

The emergence of plane channeling makes a case for the multiscale nature of short-circuiting within such geothermal systems. That is, regardless of the scale at which the system is modelled — be it a single plane, multi-plane, or discrete fracture network within the rock mass — short-circuiting will be observed at every level. By the nature of the coupled THM system, any initial configuration with multiple flow pathways is unstable, and flow in such systems is expected to always degenerate to a single dominant pathway over time, unless some process intervention is introduced.

5.3. *Bifucation of the in-plane short-circuiting mechanism*

In most cases that we have studied, the in-plane short-circuiting pathway in multi-fracture models appears to be similar to that observed in the single fracture model, described in Section 4. However, alternate equilibrium branches are observed in the 50 m fracture spacing scenarios with 18 and 20 cm well casings. These scenarios show the most interesting Plane 2 dominant flows. In these instances, a bifurcation of the short-circuiting pathway is observed due to hydro-mechanical interaction between planes. The fluid temperature, fracture aperture, and fluid velocities for the two-fracture EGS with 50 m spacing and 20 cm well casings are illustrated in Fig. 20.

At 15 months, the fractures in Fig. 20 look very similar to those of Fig. 17. As always, an in-plane short-circuit begins in Plane 2 before Plane 1 which leads to an increase in flow in Plane 2. The increase in flow is accompanied by an increase in fluid pressure. Unlike the fractures in Fig. 17, the fractures in Fig. 20 are close together such that the pressure in Plane 2 pushes against Plane 1 along the default short-circuiting path and closes the fracture aperture in this area, as shown at 25 months in Fig. 20. This prevents the development of short-circuiting in Plane 1 along the midline between wells, explaining the extended duration of Plane 2 dominant flow. The fluid in Plane 1 must therefore reroute itself around the region of closed aperture, as illustrated in the velocity contours. The fundamental THM feedback mechanism of the in-plane short-circuiting applies regardless of the path that the flow takes. The aperture along the rerouted path therefore increases, creating an open channel around the area of decreased aperture. The eventual opening of a channel in Plane 1 is illustrated in Fig. 21, where it is observed at the midline that Plane 2 is fully open while Plane 1 is closed, but offset from the midline Plane 1 is fully open between the injection and production wells. Once a short-circuit pathway opens in Plane 1, plane channeling takes over and the multi-fracture flow decays over time to Plane 1 flow.

Well casing size generally has little effect on production temperature. The bifurcated short-circuit pathway is the exception to this trend, as it causes a smearing of the transition between the quasi-steady state and short-circuiting regimes. The onset of the short-circuiting regime is governed by the first incidence of in-plane short-circuiting within the system and is therefore unaffected by the bifurcated pathway.

The bifurcation of the fluid pathway only occurs due to the right combination of fracture spacing, casing diameter, and initial hydraulic aperture. It is possible that bifurcation of the short-circuiting pathway may emerge at larger fracture spacings, but would require both smaller initial hydraulic apertures and smaller well casing diameters to increase fluid pressure and overcome the increased stiffness of the rock mass. The bifurcation of short-circuiting pathways is only observed when considering fully-coupled THM behaviour of the system with hydraulically connected fractures. The existence of multiple short-circuiting pathways speaks to the complex THM nature of short-circuiting and the potential generalization of these findings to non-homogeneous fracture planes.

6. Implications for EGS projects

In this model, the rock mass is assumed to have homogeneous isotropic properties, and the fracture apertures have been assumed to be uniform. These are simplifying assumptions, as true rock masses are anisotropic and highly heterogeneous. The fracture apertures will also not be uniform, perhaps consisting of a highly heterogeneous and tortuous network of smaller fracture pathways. Furthermore, there will be self-propping effects because of fracture surface roughness, partial irreversibility of aperture opening in all cases, and the potential placement of proppant during the formation stimulation activity to connect the wells. The behaviour and performance of the homogeneous systems studied here are thus not necessarily representative of the heterogeneous conditions present in a rock mass. Nonetheless, if homogenous

systems exhibit short-circuiting, then we may surmise that it is of concern in reservoirs that are naturally fractured and heterogeneous. The observed short-circuiting mechanisms are products of the THM coupling of the system. The behaviour and production temperature curves from homogeneous fractures are most likely a best-case, and poorer responses may be expected in the presence of heterogeneity and fracture complexity. Previous studies which have examined the role of heterogeneities and heat recovery have shown more a rapid decline in heat production compared to the homogeneous case (Guo et al., 2016), and we have a similar expectation for the systems studied here.

The EGSs studied here show short-circuiting within 36 months for a single fracture EGS and 12–24 months for a multi-fracture EGS. There is evidence from the field to support these findings, as short-circuiting was also observed within 12 months of operation during the long-term circulation test at the Hijori Hot Dry Rock test site (Yanagisawa et al., 2008; Tenma et al., 2008). It is reasonable to ask: can short-circuiting be expected early-on in the operation of any EGS project? The answer seems to be no. In a previous study of a deep EGS system (based on the Habanero project) with larger in-situ stress ($\sigma_{hmin} = 70$ MPa, $\sigma_{Hmax} = 100$ MPa and $\sigma_V = 64$ MPa), lower injection rate (12.5 L/s), and larger distance between wells (500 m) did not show any short-circuiting after 30 years of injection (Guo et al., 2016; Slatlem Vik et al., 2018). In Gee and Gracie (2021), we were able to confirm the results of Guo et al. (2016), using the same simulator used in this manuscript. Although short-circuiting was not observed, THM effects still had a significant impact on the production temperature (Guo et al., 2016; Gee and Gracie, 2021). These previous studies of deep EGSs differ from the relatively shallow EGSs studied here in which in-situ stresses are lower ($\sigma_{hmin} = 26$ MPa, $\sigma_{Hmax} = 31$ MPa and $\sigma_V = 39$ MPa), the injection rate is higher (50 L/s), and the wells are more closely spaced (250 m). Thus, whether short-circuiting can be expected early-on in the operation of an EGS depends both on the EGS reservoir characteristics (e.g., in-situ stresses) and operational considerations (e.g., injection rate and well spacing).

While short-circuiting has negative implications for the long-term viability of an EGS, the model considered does not account for the creation and opening of tensile daughter fractures normal to the dominant planes due to thermal contraction. Daughter fractures would increase the ability of the rock mass to distribute thermal strain without increasing fracture aperture, in addition to increasing the surface area over which heat transfer occurs, and so may have a positive influence on the EGS behaviour.

The ability to withdraw energy from the reservoir prior to creating a short-circuit may also be improved through design by optimizing parameters such as injection rate, injection temperature, and well spacing. Furthermore, intelligent operation of the wells may improve the viability of an EGS. The multi-scale omnipresent nature of short-circuiting lends favourability to the design philosophy of zoning, in which short-circuiting is accepted as an inevitability. With zoning, production is staggered through the different fractures, and flow controls are introduced to manually partition flow between the fracture planes. Production can then switch from one fracture to the next when short-circuiting occurs in the current fracture.

7. Conclusions

In this article, the short-circuiting mechanisms within single and multi-fracture enhanced geothermal systems are explored. EGS well doublets are simulated using a fully-coupled thermo-hydro-mechanical finite element model in which flow is restricted to dominant fracture planes which are hydraulically connected by the injection and production wells.

It is demonstrated that within the range of common material and design parameters, only the transient behaviour of the rock temperature needs to be modelled, while all other fields can be assumed static or steady-state. Short-circuiting is demonstrated to be a multi-scale phenomenon within an EGS system, and both in-plane and inter-plane short-circuiting mechanisms have been observed. The in-plane short-circuiting mechanism, flow channeling, dominates the overall production temperature of the system. The development of flow channeling has been characterised using production flow regimes which correspond to the development of specific phenomena within a fracture plane. It is demonstrated that flow channeling is worse in multi-fracture reservoirs because of the increased amount of thermal contraction that occurs between the fracture planes. Two reservoir-scale inter-plane short-circuiting mechanisms are described for the first time: plane channeling, and bifurcation of the short-circuiting pathway. These inter-plane short-circuiting mechanisms are shown to have large impacts on the distribution of flow throughout the reservoir, but relatively little impact on the overall production temperature response of the studied systems.

The implications of these short-circuiting mechanisms as they apply to naturally fractured rock masses are important. Future work on EGS reservoirs will consist of exploring design and production strategies to mitigate the development of short-circuiting within the system, as well as exploring the effectiveness of zoning to increase the overall production life of an EGS project.

Author contributions

Bruce Gee: Methodology, Software, Investigation, Formal Analysis, Writing – Original Draft, Visualisation

Robert Gracie: Methodology, Resources, Supervision, Writing – Reviewing and Editing, Project Administration

Maurice Dusseault: Conceptualization, Writing – Reviewing and Editing

Conflict of interest

The authors declare no conflict of interest.

Declaration of Competing Interest

The authors report no declarations of interest.

Acknowledgements

Dr. Gracie acknowledges the support of a Discovery Grant from the Natural Sciences and Engineering Research Council of Canada (NSERC), as well as an Early Researcher Award from the Ontario Ministry of Research and Innovation. Bruce Gee acknowledges the support of an Alexander Graham Bell Graduate Scholarship from NSERC, as well as an Engineering Excellence Fellowship from the University of Waterloo. We all thank the University of Waterloo for encouragement in research and education.

Appendix A. Aperture development at the production well

The growth of aperture at the production well is driven by different physical behaviour than the injection well. Aperture at the injection well increases due to thermal contraction (uniform cooling), while aperture at the production well increases due to differential thermal contraction at a sharp thermal front (non-uniform cooling). In this appendix, the behaviour of the aperture growth at the production well is examined through a simplified two-dimensional analogous situation. In the full simulated rock mass, the behaviour is complicated by the fluid pressure, in-situ stresses, the three-dimensional temperature distribution, and contact with the opposite face of the fracture. In this simplified simulation, the thermo-mechanical deformation of a two-dimensional sharp thermal front is examined without any other external applied forces. This simplified analogous situation demonstrates that the behaviour of increased aperture at the production well can be attributed to the effects of thermal contraction at a sharp temperature front.

Consider the thermo-mechanical deformation of the two domains illustrated in Figs. A.22a and b. The domain in Fig. A.22a is subject to thermal contraction in a thin strip along the entire width of the domain, analogous to the approximately uniaxial local temperature distribution around the injection well. The domain in Fig. A.22b is subject to thermal contraction in a thin strip that only extends half the width of the domain, simulating the sharp thermal front observed near the production well. Placement of the vertically constrained node has no impact on the phenomena demonstrated. The material parameters of the domains are listed in Table A.3, and are the same as the rock masses simulated in Sections 4 and 5. The domains are subject to the same thermal contraction of $\Delta\theta = -140\,^{\circ}\mathrm{C}$, which is approximately the same temperature difference experienced by the simulated rock masses.

The deformation of the two-dimensional domains under the thermal contraction are illustrated in Figs. A.23a and b. As illustrated in Fig. A.23b, the non-uniform contraction induces rigid body rotation in the rock mass. Any two horizontally adjacent points in a constrained body which do not experience the same amount of thermal strain will induce shear, and since the domains are horizontally constrained, this shear induces rotation. Rotation leads to the creation of larger displacements compared to the first case illustrated in Fig. A.23a, in which the deformation is uniaxial. Thus, it is demonstrated how differential thermal contraction at a sharp thermal front can lead to the development of greater apertures.

There is a rotation of the body associated with any thermal front, but the reason that the increased apertures are only observed near the production well is because the temperature front is sharp at the production well but diffuse elsewhere. As illustrated by the fluid temperature contours in Fig. 12, there is an abrupt change in the temperature at the production well: the temperature on the side of the injection well is cold (about 80 °C), while on the far side of the production well the temperature returns to 225 °C within 5 m. The steep temperature gradient creates larger rotation. Elsewhere in the domain, the temperature gradients are much smaller, moving gradually from cold to hot over lengths of 50–400 m. Where the temperature change is less abrupt, the relative difference in the amount of contraction experienced by any two adjacent points in the rock mass is smaller, which reduces the shear and rigid body rotation of the rock mass.

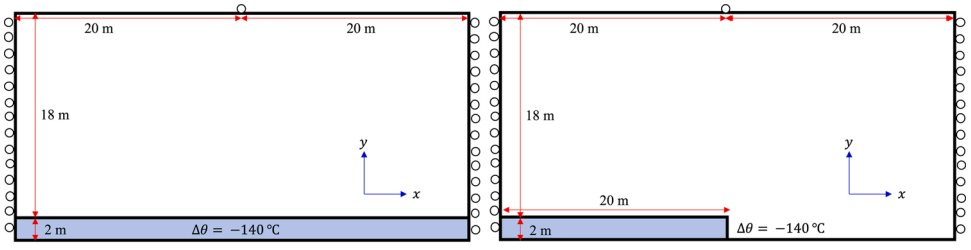

(a) Full width contraction (b) Sharp thermal front contraction

Fig. A.22. Two-dimensional domains with temperature distributions analogous to the injection and production wells.

Table A.3
Material parameters of two-dimensional domains.

Parameters	Variable	
Elastic modulus	E	59 GPa
Poisson's ratio	ν	0.28
Coefficient of thermal expansion	α	8×10^{-6} m/m °C

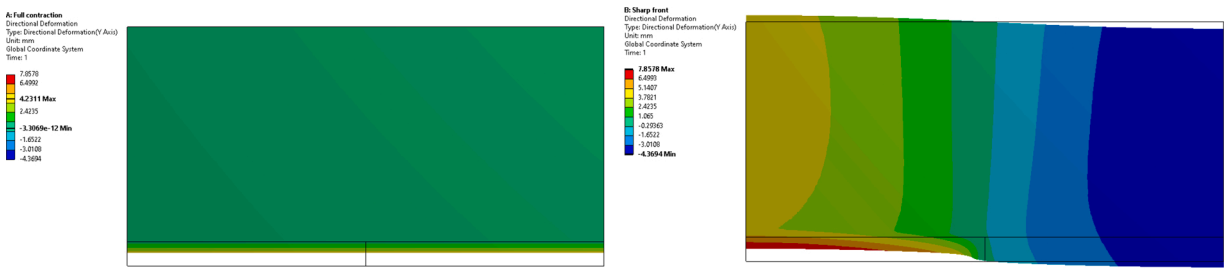

(a) Full width contraction. $u_{ymax} = 4.2$ mm (b) Sharp thermal front contraction. $u_{ymax} = 7.9$ mm

Fig. A.23. Vertical deformation of the two-dimensional domains with temperature distributions analogous to the injection and production wells.

References

Aliyu, M.D., Chen, H.-P., 2018. Enhanced geothermal system modelling with multiple pore media: thermo-hydraulic coupled processes. Energy 165, 931–948. https://doi.org/10.1016/j.energy.2018.09.129.

Asai, P., Panja, P., Velasco, R., Mclennan, J., Moore, J., 2018. Fluid flow distribution in fractures for a doublet system in Enhanced Geothermal Systems (EGS). Geothermics 75 (C), 171–179.

Bejan, A., 2013. Convection Heat Transfer, 4th Edition. Wiley, Hoboken, NJ.

Brooks, A.N., Hughes, T.J., 1982. Streamline upwind/Petrov-Galerkin formulations for convection dominated flows with particular emphasis on the incompressible Navier-Stokes equations. Comput. Methods Appl. Mech. Eng. 32 (1–3), 199–259.

Chen, Y., Ma, G., Wang, H., Li, T., 2018. Evaluation of geothermal development in fractured hot dry rock based on three dimensional unified pipe-network method. Appl. Therm. Eng. 136, 219–228.

Colebrook, C.F., 1939. Turbulent flow in pipes, with particular reference to the transition region between the smooth and rough pipe laws. J. Inst. Civil Eng. 11 (4), 133–156. https://doi.org/10.1680/ijoti.1939.13150.

Faragó, I., Horváth, R., 2007. A review of reliable numerical models for three-dimensional linear parabolic problems. Int. J. Numer. Methods Eng. 70 (1), 25–45.

Fu, P., Hao, Y., Walsh, S., Carrigan, C., 2016. Thermal drawdown-induced flow channeling in fractured geothermal reservoirs. Rock Mech. Rock Eng. 49 (3), 1001–1024.

Gan, Q., Elsworth, D., 2016. Production optimization in fractured geothermal reservoirs by coupled discrete fracture network modeling. Geothermics 62, 131–142. https://doi.org/10.1016/j.geothermics.2016.04.009.

Gee, B., Gracie, R., 2021. Comparison of fully-coupled and sequential solution methodologies for enhanced geothermal systems. Comput. Methods Appl. Mech. Eng. 373, 113554. https://doi.org/10.1016/j.cma.2020.113554.

Ghassemi, A., Zhou, X., 2011. A three-dimensional thermo-poroelastic model for fracture response to injectionextraction in enhanced geothermal systems. Geothermics 40 (1), 39–49.

Gong, F., Tiankui, G., Sun, W., Li, Z., Bin, Y., Chen, Y., Qu, Z., 2020. Evaluation of geothermal energy extraction in Enhanced Geothermal System (EGS) with multiple fracturing horizontal wells (MFHW). Renew. Energy 151, 1339–1351. https://doi.org/10.1016/j.renene.2019.11.134.

Grasby, S., Allen, D., Bell, S., Chen, Z., Ferguson, G., Jessop, A., Kelman, M., Ko, M., Majorowicz, J., Moore, M., Raymond, J., Therrien, R., 2013. Geothermal Energy Resource Potential of Canada, Geological Survey of Canada Open File; 6914. Geological Survey of Canada, Ottawa, Ont.

Guo, B., Fu, P., Hao, Y., Peters, C.A., Carrigan, C.R., 2016. Thermal drawdown-induced flow channeling in a single fracture in EGS. Geothermics 61 (C), 46–62.

Han, S., Cheng, Y., Gao, Q., Yan, C., Zhang, J., 2020. Numerical study on heat extraction performance of multistage fracturing enhanced geothermal system. Renew. Energy 149, 1214–1226. https://doi.org/10.1016/j.renene.2019.10.114.

Harari, I., 2004. Stability of semidiscrete formulations for parabolic problems at small time steps. Comput. Methods Appl. Mech. Eng. 193 (15–16), 1491–1516.

Heuze, F., 1983. High-temperature mechanical, physical and thermal properties of granitic rocks – a review. Int. J. Rock Mech. Min. Sci. Geomech. Abstr. 20 (1), 3–10.

Küttler, U., Wall, W., 2008. Fixed-point fluid-structure interaction solvers with dynamic relaxation. Comput. Mech. 43 (1), 61–72.

Kinney, C., Dehghani-Sanij, A., Mahbaz, S., Dusseault, M., Nathwani, J., Fraser, R., 2019. Geothermal energy for sustainable food production in Canada's remote northern communities. Energies (Basel) 12 (21), 4058.

Kolditz, O., Görke, U.-J., Shao, H., Wang, W., 2012. Thermo-Hydro-Mechanical-Chemical Processes in Porous Media: Benchmarks and Examples, Vol. 86 of Lecture Notes in Computational Science and Engineering. Springer Berlin Heidelberg, Berlin, Heidelberg.

Mohais, R., Xu, C., Dowd, P., 2011. Fluid flow and heat transfer within a single horizontal fracture in an enhanced geothermal system. J. Heat Transf. 133 (11).

Pandey, S., Chaudhuri, A., Kelkar, S., 2017. A coupled thermo-hydro-mechanical modeling of fracture aperture alteration and reservoir deformation during heat extraction from a geothermal reservoir. Geothermics 65, 17–31.

Peirce, A., Detournay, E., 2008. An implicit level set method for modeling hydraulically driven fractures. Comput. Methods Appl. Mech. Eng. 197 (33–40), 2858–2885.

Salimzadeh, S., Nick, H., 2019. A coupled model for reactive flow through deformable fractures in Enhanced Geothermal Systems. Geothermics 81, 88–100.

Salimzadeh, S., Nick, H.M., Zimmerman, R., 2018a. Thermoporoelastic effects during heat extraction from low-permeability reservoirs. Energy 142, 546–558.

Salimzadeh, S., Paluszny, A., Nick, H.M., Zimmerman, R.W., 2018b. A three-dimensional coupled thermo-hydro-mechanical model for deformable fractured geothermal systems. Geothermics 71, 212–224.

Shaik, A.R., Rahman, S.S., Tran, N.H., Tran, T., 2011. Numerical simulation of fluid-rock coupling heat transfer in naturally fractured geothermal system. Appl. Therm. Eng. 31 (10), 1600–1606.

Slatlem Vik, H., Salimzadeh, S., Nick, H.M., 2018. Heat recovery from multiple-fracture enhanced geothermal systems: the effect of thermoelastic fracture interactions. Renew. Energy 121, 606–622.

Somerton, W.H., 1992. Thermal Properties and Temperature-Related Behavior of Rock/Fluid Systems, Developments in Petroleum Science, vol. 37. Elsevier, Amsterdam.

Tenma, N., Yamaguchi, T., Zyvoloski, G., 2008. The Hijiori Hot Dry Rock test site, Japan: evaluation and optimization of heat extraction from a two-layered reservoir. Geothermics 37 (1), 19–52. https://doi.org/10.1016/j.geothermics.2007.11.002.

U.S. D. of Energy, 2020. Utah FORGE Numerical Modelling (accessed 10.06.20). https://utahforge.com/laboratory/numerical-modeling.

Walsh, S.D., Garapati, N., Leal, A.M., Saar, M.O., 2017. Calculating thermophysical fluid properties during geothermal energy production with NESS and Reaktoro. Geothermics 70, 146–154.

Wang, G., Liu, G., Zhao, Z., Liu, Y., Pu, H., 2019a. A robust numerical method for modeling multiple wells in city-scale geothermal field based on simplified one-dimensional well model. Renew. Energy 139, 873–894.

Wang, Y., Li, T., Chen, Y., Ma, G., 2019b. A three-dimensional thermo-hydro-mechanical coupled model for enhanced geothermal systems (EGS) embedded with discrete fracture networks. Comput. Methods Appl. Mech. Eng. 356, 465–489.

Xia, Y., Plummer, M., Mattson, E., Podgorney, R., Ghassemi, A., 2017. Design, modeling, and evaluation of a doublet heat extraction model in enhanced geothermal systems. Renew. Energy 105, 232–247. https://doi.org/10.1016/j.renene.2016.12.064.

Xie, L., Min, K.-B., Song, Y., 2015. Observations of hydraulic stimulations in seven enhanced geothermal system projects. Renew. Energy 79.

Yanagisawa, N., Matsunaga, I., Sugita, H., Sato, M., Okabe, T., 2008. Temperature-dependent scale precipitation in the Hijiori Hot Dry Rock system, Japan. Geothermics 37 (1), 1–18.

Zeng, Y.-C., Su, Z., Wu, N.-Y., 2013. Numerical simulation of heat production potential from hot dry rock by water circulating through two horizontal wells at Desert Peak geothermal field. Energy 56, 92–107. https://doi.org/10.1016/j.energy.2013.04.055.

Zhang, W., Qu, Z., Guo, T., Wang, Z., 2019. Study of the enhanced geothermal system (EGS) heat mining from variably fractured hot dry rock under thermal stress. Renew. Energy 143, 855–871.